

**Analysis of non-coding RNA expression in medium spiny neurons
of Huntington disease model mice**

DOCTORAL DISSERTATION

A thesis submitted in partial fulfillment of the requirements
for the degree of Doctor of Philosophy

By:

Hongsun Park

Supervisor:

Dr. Nobuyuki Nukina

Co-Supervisors:

Dr. Haruko Miyazaki

Dr. Tomoyuki Yamanaka

Graduate School of Brain Science

Doshisha University

March 2019

Kyoto, Japan

Table of Contents

Abstract	4
Acknowledgement.....	5
Chapter 1. Introduction	6
1.1. Huntington disease (HD).....	6
1.2. Huntingtin gene, huntingtin protein and polyglutamine.....	7
1.3. The pathomechanism of HD	10
1.4. HD mouse models	12
1.5. Non-coding RNAs in neurodegenerative diseases	13
Chapter 2. Materials and Methods	16
Chapter 3. Results.....	23
3.1. Dysregulated ncRNAs were found in the gene expression profiling data of R6/2 MSN	23
3.2. NcRNA expressions were altered, confirmed by qRT-PCR	24
3.3. The dysregulation of ncRNA could not be confirmed by ISH	26
3.4. NcRNA with low expression level was detected by ViewRNA ISH.	27
3.5. Non-coding RNA <i>Abhd11os</i> and <i>Neat1</i> were downregulated in R6/2.....	30
3.6. <i>Abhd11os</i> and <i>Neat1</i> in MSN was downregulated in R6/2	32
3.7. Dysregulation of <i>Neat1</i> might affect the morphology of paraspeckles	40
Chapter 4. Discussion	42
4.1. Non-coding RNA <i>Abhd11os</i> and HD	42
4.2. Non-coding RNA <i>Neat1</i> , paraspeckles and HD.....	43
4.3. The effectiveness of ViewRNA ISH compared to the conventional ISH.....	45
4.4. Future perspectives.....	45
Chapter 5. References	47

Table of Figures

Table 1. Primers for qRT-PCR	17
Table 2. 12 ncRNAs that were dysregulated in MSN of 4-week-old HD model mouse brains	24
Figure 1. Schematic diagram of huntingtin protein (htt).....	8
Figure 2. Schema of R6/2 Venus mouse generation and microarray analysis.....	16
Figure 3. Construction of cRNA probe for ISH.....	19
Figure 4. Workflow of ViewRNA ISH	21
Figure 5. Verification of dysregulated ncRNAs in R6/2 striatum and MSN.....	25
Figure 6. Two variants of <i>Neat1</i> : <i>Neat1-1</i> and <i>Neat1-2</i>	26
Figure 7. NcRNAs could not be detected by conventional ISH.....	27
Figure 8. ViewRNA ISH allowed to detect ncRNA with low expression level.....	28
Figure 9. ViewRNA ISH allows for precise localizations of <i>Scn4b</i>	29
Figure 10. The signals of <i>Abhd11os</i> and <i>Neat1</i> were detected by ViewRNA ISH.....	31
Figure 11. Quantification of dotted signals of <i>Abhd11os</i> and <i>Neat1</i> in R6/2 striatum	32
Figure 12. Mutant huntingtin is present in MSN of 4-week-old R6/2	33
Figure 13. <i>Abhd11os</i> signals in MSN were reduced in R6/2	36
Figure 14. The signals of <i>Neat1-1</i> and <i>Neat1-2</i> in MSN were decreased in R6/2.....	37
Figure 15. The signals of <i>Neat1-1</i> and <i>Neat1-2</i> localized with paraspeckles were reduced in R6/2.....	39
Figure 16. PSF positive signals seemed to be more dispersed in R6/2.....	41

Abstract

Huntington Disease (HD) is an inherited neurodegenerative disorder with symptoms of movement disorders, psychiatric disturbances and dementia. The disease is caused by expanded CAG repeats encoding polyglutamine in the exon1 of huntingtin gene (*HTT*). In the brains of HD patients, the mutant *HTT* affects the transcriptional profile of neurons by disrupting the activities of transcriptional machinery which alters the expression of many genes. Neurodegeneration is most pronounced in the striatum, and medium spiny neurons (MSN) are lost.

In this study, we identified dysregulated non-coding RNAs (ncRNAs) that have homology with human ncRNAs from the gene expression profiling data of MSN in 4-week-old R6/2 HD model mice. By performing real-time PCR, we examined the expression levels of these ncRNAs in the striatum and MSN of R6/2 and control mouse. Also, we observed the intracellular localizations of *Abhd11os* and *Neat1* ncRNAs by ViewRNA ISH, which provides more precise detection, suggesting that ViewRNA ISH may be a useful method to investigate the expression changes in the expression of genes with low expression levels.

Acknowledgement

Firstly, I would like to express my deepest appreciation to my advisors, Dr. Nobuyuki Nukina, Dr. Haruko Miyazaki, and Dr. Tomoyuki Yamanaka, for their invaluable support and for providing their insight and expertise which greatly improved this study. I would also like to give special thanks to my dissertation committee, Dr. Fumino Fujiyama, Dr. Jun Motoyama, and Dr. Shigeo Takamori, for their advice, encouragement, and constructive criticism that motivated me to broaden my perspectives in regard to my research.

This work would not have been possible without the financial support of the Ministry of Education, Culture, Sports, Science and Technology (MEXT) and Doshisha University.

I am also thankful to my friends and the lab members for encouraging and supporting me through this entire process. In particular, I thank Edward William Ko Uy for editing English of this manuscript.

Finally, I must express my very profound gratitude to my parents and my sister who have always been supportive throughout my years of study and my life in general. This dissertation stands as a testament to their unconditional love and encouragement.

Chapter 1. Introduction

1.1. Huntington disease (HD)

Huntington disease (HD) is a dominantly-inherited disorder that was first described in 1872 by the American physician George Huntington. The incidence of HD is variable across the globe, ranging from around 0.5 per 100,000 people of Japanese and Chinese to more than 10 per 100,000 people of European ancestry. Additionally, there is a high prevalence of HD patients living by the shores of Lake Maracaibo, Venezuela (700 per 100,000). This particular population was recognized by Hereditary Disease Foundation and later helped in mapping and isolation of HD gene, leading to the initiating of molecular research in HD (Pandey and Rajamma, 2018, Wexler et al., 2004). The disease is fatal approximately 15 to 20 years after the age of onset, and the age of onset distribution in HD is broad and may vary from as young as age 2 or 3 and as old as age 80 or more (Myers, 2004). The most common form of this disorder is adult-onset HD, the age at onset of which appears in a person's thirties and forties, and the symptoms become more pronounced as the disease progresses.

HD, originally termed as "Huntington's chorea", is mainly classified as a movement disorder since the disease causes the motor symptoms including chorea (involuntary writhing movements), dystonia (involuntary contraction of muscles) and dyskinesia (disability of performing voluntary movements). However, HD also causes psychiatric disturbances including depression, anxiety and irritability and cognitive impairments leading to dementia. Along these behavioral features, the neuropathological features of HD have been reported. One of the key neuropathological features of HD is a selective loss of medium spiny neurons (MSN) in the striatum (Zuccato et al., 2010). Also, HD brains weigh 10-20% less than age-matched control brains caused by neuronal loss, resulting in the smaller brain size in the late stage of the disease compared to the controls (Pandey and Rajamma, 2018).

Despite a number of researches for HD pathogenesis, the treatment of the disease has still been elusive. In order to reduce involuntary movements, treatments that reduce the actions of dopamine in the basal ganglia such as haloperidol, a conventional dopamine antagonist, have been suggested and used. However, the long-term use of these treatments showed side effects such as Parkinson-like symptoms. Therefore, tetrabenazine, the only treatment approved by the U.S. Food and Drug Administration (FDA) so far to treat chorea caused by HD, has been considered as an alternative and is widely used with less side effects. For the psychiatric and cognitive symptoms, no adequate treatments have been reported. In addition, most HD patients experience weight loss caused by dysphagia, difficulty in swallowing, in which swallowing therapy can help (Wexler, 2012).

1.2. Huntingtin gene, huntingtin protein and polyglutamine

In 1983, a genetic marker was first located near the telomere (or tip) of the short arm of chromosome 4 (Gusella et al., 1983). It took another ten years for the gene to be identified as huntingtin gene (*HTT*) in which the CAG repeat in the exon1 is expanded (The Huntington's Disease Collaborative Research Group, 1993). This gene produces a protein called huntingtin (*htt*) that is found ubiquitously throughout the body with the highest levels in the CNS (Fusco et al., 1999). The normal range of the CAG repeat is about 6-35, but in HD, it expands from 36 to more than 120 (Bauer and Nukina, 2009). The HD patients have *htt* with expanded CAG repeats, which translate into polyglutamine (polyQ), at the exon1 of *HTT* gene (**Figure 1**). As the number of CAG repeat increases, the age of disease onset becomes earlier. At least four repeated polyQ repeats are observed in all vertebrates with the number of polyQ increasing in higher species, the longest polyQ tract found in humans (Schulte and Littleton, 2011).

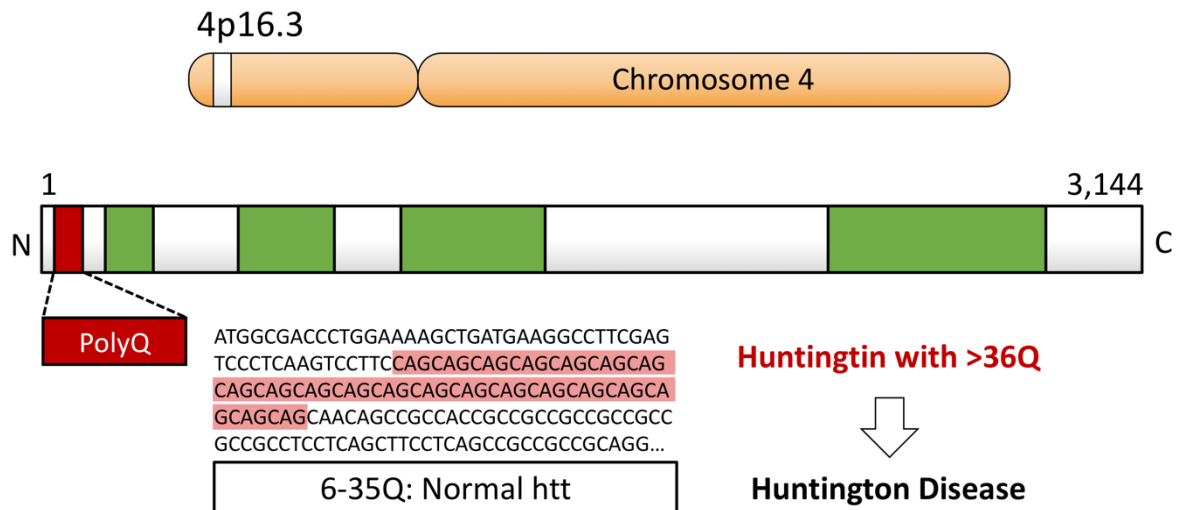


Figure 1. Schematic diagram of huntingtin protein (htt)

HTT gene is mapped on the short arm of chromosome 4 (4p16.3). The CAG repeat in the exon1 of *HTT* is expanded, encoding polyQ (red box). Htt contains HEAT repeats (green box), and the number of amino acids of normal htt is 3,144. Abnormal htt with more than 36 glutamines leads to Huntington disease.

Although it has been decades since the gene was identified, the exact function of htt is still unclear though its function has been speculated based on its structure. Htt is a completely soluble protein of 3,144 amino acids with many potential domains such as HEAT (Huntingtin, Elongation factor 3A, a subunit of Protein Phosphatase 2A and the yeast kinase TOR1) repeats that have not been fully understood (**Figure 1**). All Htt orthologs with similar sizes contain HEAT repeats which are conserved in vertebrates and are thought to mediate protein-protein interactions (Takano and Gusella, 2002). This indicates that htt may interact with similar proteins across vertebrates. Also, it is reported that htt is palmitoylated at C214 by its co-partner, HIP14 (htt-interacting protein 14), but the precise amino acid position involved is unknown. The polyQ expansion of htt results in a reduction of the enzymatic activity of HIP14 and the autopalmitoylation of htt (Huang et al., 2011), leading to changes in the intracellular trafficking and synaptic localization of other neuronal proteins. This is consistent with other palmitoylated proteins which are often involved in the dynamic assembly of components that control vesicle

trafficking and synaptic vesicle function (DiFiglia et al., 1995). Intracellularly, htt is associated with various organelles, including the nucleus, endoplasmic reticulum and Golgi complex, and it is also found in neurites and at synapses, but this widespread localization does not explain their function (Cattaneo et al., 2005). Despite the lacking evidence, htt is regarded as an essential protein for embryonic development because the disruption of htt (*Hdh*^{-/-}) in mice causes embryonic death before day 8.5 when gastrulation and the formation of the nervous system begin (Nasir et al., 1995).

To confirm whether the polyQ stretch plays a crucial role during embryonic development, a study investigated the impact of deleting the polyQ stretch on the normal function of a vertebrate htt (Clabough and Zeitlin, 2006). In order to examine the contribution of the polyQ stretch to normal htt function *in vivo*, the researchers generated mice with a precise deletion of the (CAG)₂CAA(CAG)₄ triplet repeat encoding 7Q within the mouse homolog of the HD gene (*Hdh*^{ΔQ}). They found that the polyQ stretch is not essential for normal htt function during development since the survival of *Hdh*^{ΔQ/ΔQ} pups were not affected at birth. However, *Hdh*^{ΔQ/ΔQ} homozygous adult mice commit more errors initially in a learning and memory test but perform slightly better than wild-type controls in the accelerating rotating rod test for motor coordination. Also, they found that primary fibroblasts obtained from embryos homozygous for the ΔQ deletion exhibit elevated levels of ATP but aged more rapidly than wild-type controls. Taking these results together, the researchers suggested that the polyQ stretch within htt is required for modulating longevity in primary cell culture and that one of htt's normal functions may also be involved in regulating energy homeostasis in vertebrates.

In addition, wild-type htt has also been associated to brain-derived neurotrophic factor (BDNF), which is particularly important for the survival of striatal neurons and the activity of cortico-striatal synapses. BDNF is co-localized with htt in cortical neurons that project to the striatum, and most striatal BDNF is produced in the cerebral cortex. These cortical BDNF, which are transported anterogradely in vesicles along the cortico-striatal afferents, are released

at the axon terminals and captured by striatal neurons, giving rise to rapid intracellular signals. BDNF also controls glutamate release, and its exogenous administration allows striatal neurons to survive excitotoxin-induced neurodegeneration (Cattaneo et al., 2005). It is reported that wild-type htt stimulates these cortical BDNF production by acting at the level of *Bdnf* gene transcription. Cultured brain cells overexpressing wild-type htt produce increased BDNF mRNA and protein, an effect lost in cells overexpressing mutant htt (Zuccato et al., 2001). Furthermore, mutant htt causes a similar reduction in the transcription of BDNF mRNA and also decreases transcription from *Bdnf* exons III and IV (Zuccato et al., 2003), suggesting that the reduced cortical BDNF levels in HD are due to both the loss of wild-type htt function and increased toxicity of the mutant htt. These findings suggest that htt contributes to the pool of BDNF protein produced in the cerebral cortex. Also, htt may regulate BDNF transport along the cortico-striatal afferents with the mutation of the protein affecting the ability of BDNF to reach its striatal targets.

1.3. The pathomechanism of HD

HD is considered as one of the so-called polyglutamine diseases. The polyQ tract in htt can also lead to a type of protein bundling known as nuclear inclusions (NI). An enzyme cuts htt into small fragments which are able to enter the nuclei of neurons. In experiments, the truncated molecules of htt form the highest number of polyQ-containing aggregates in neurons *in vitro* and lead to the earliest and the most severe behavioral disorders in transgenic mice *in vivo* (Ross et al., 1999).

When analyzing neurotoxicity and developing approaches for molecular therapy in HD, it is necessary to clearly differentiate the most pathogenic polyQ-containing fragments and their final product, NIs. Although it seems obvious that NI formation is a natural phenomenon in the progress of HD, the cause-effect relationships between the presence of inclusions and the neuronal degeneration has not been fully understood. Previous studies have observed a

certain dissociation between the number of inclusions and the intensity of neurodegeneration in transgenic mice expressing expanded CAG repeats (Davies et al., 1997) and in the HD cell models (Saudou et al., 1998, Kim et al., 1999). These findings support the idea that the formation of intracellular polyQ-containing inclusions is an epiphenomenon of a parallel pathological process. However, current studies about the pathomechanism of polyglutamine diseases in humans and mouse models suggest a two-stage model of pathogenesis, the prolonged period of neuronal dysfunction followed by the relatively short period of neuronal loss. Therefore, it is important to discover mechanisms of neurotoxicity of polyQ-containing protein molecules during the early stage of their expression. Until now, several mechanisms have been suggested: dysregulation of transcription, disorders in the mitochondria functions and in the energy metabolism, defects of the cytoskeleton and axonal transport, induction of neuroimmune inflammatory reactions, oxidative stress and loss of own physiological functions of htt (Illarioshkin et al., 2018). In this study, we focused on the dysregulation of transcription in HD.

To possess its neurotoxicity, the mutant htt (mHtt) has to be translocated within the nuclei, and the neurodegenerative cascade in HD is initiated after the nuclear translocation of the htt fragments in neurons, which is now considered as the earliest link in the molecular pathogenesis of HD. The N-terminal fragments of mHtt, caused by abnormal alternative splicing of the *HTT* mRNA, flow into nuclei and disrupt the activities of transcriptional machinery such as transcriptional factors (Luthi-Carter et al., 2002, Chan et al., 2002). For example, CBP, CREB-binding protein, is present in polyQ nuclear aggregates in HD cell culture models, transgenic mice (Htt-N171-82Q) and human HD postmortem brains. Control brains do not contain inclusions, and CBP has a diffuse distribution in nuclei. This suggests that mHtt specifically interferes with CBP-mediated transcription through the interaction with polyQ aggregates (Nucifora et al., 2001). Another example is NF-Y, which also colocalizes with ubiquitin-positive nuclear inclusions in cortex and striatum of HD model mouse. It was

suggested that this abnormal localization of NF-Y affects the activities and expression of HSP70 (Yamanaka et al., 2008). Taking these together, mutant *HTT* may disrupt the activities of transcription factors and alter expression of many genes in HD. This has been investigated in the post-mortem brains from HD patients and animal models, therefore, from the functional viewpoint, HD can also be considered as transcription pathologies (Illarioshkin et al., 2018).

1.4. HD mouse models

In 1996, Mangiarini et al. generated lines of mice (R6) that are transgenic for the HD mutation (Mangiarini et al., 1996). The transgene contains 1kb of the human HD promoter region, exon1 carrying CAG repeat expansions ranging from 115-156 repeats, and 262 bp of intron1. Among three lines, R6/2 line is used most widely for the study of HD because this line develops a progressive neurological phenotype and has been characterized most extensively. The R6/2 mice carry CAG repeat expansions ranging from 141 to 157 repeats with an age of onset of approximately 2 months. The progression of the disease is rapid, and the mice deteriorate over the following month. Behavioral motor deficits can be observed as early as 5-6 weeks of age, however overt behavioral abnormalities do not appear until 8 weeks of age, and these are followed by an early death at 10-13 weeks. The body weight of the R6/2 males decreases steadily from 8 weeks, and at 12 weeks, they weigh approximately 60% of littermate controls. Also, the brains of R6/2 mice weigh 20% less than those of littermate controls at 12 weeks, but neuronal death is minimal and delayed compared with the behavioral symptoms. NIs were initially discovered in this mouse model, preceded by the nuclear translocation of *htt* (Davies et al., 1997). In R6/2, NIs were observed densely in almost all regions of the brain.

Through a study based on this mouse model, researchers reported that numerous changes in gene expression were apparent at early stages (6 weeks) when mice showed minimal motor disorders. The researchers analyzed the changes in gene expression at different stages of the disease using DNA microarray and suggested that this expression change is secondary to an initial neuronal dysfunction (Luthi-Carter et al., 2000). By comparing the time-courses

of cell death and behavioral abnormalities, it was indicated that neuronal dysfunction is prior to neuronal death in these mice. However, the link between changes in expression levels of a selected panel of genes and the cellular dysfunction that leads to behavioral abnormalities still remains obscure.

Previous studies have revealed that human HD patients and mouse models show significant alterations in brain mRNA levels by performing large-scale microarray analyses (Augood et al., 1996, Hodges et al., 2006). For example, mRNA of $\beta 4$, the voltage-gated sodium channel, was found to be reduced significantly in the striatum of HD model mouse, R6/2, at an early stage of development (by 45% at 4 weeks, 85% at 8 weeks and 91% at 12 weeks) (Oyama et al., 2006). To investigate the alteration of gene expression in MSN directly, Venus expressed R6/2 HD model mouse was generated by crossing R6/2 and the transgenic mice with the fluorescent marker, Venus, under the control of the *Scn4b* promoter (*Scn4b-Venus*) that visualizes the cell bodies and axons of striatal projection neurons (Miyazaki et al., 2014). According to the result of FACS-array analysis, many coding and non-coding RNAs (ncRNAs) showed dysregulation in MSN of R6/2 brains. Among hundreds, those genes with fold change >1.5 , p -value <0.01 for coding RNAs and <0.05 for ncRNAs, and raw signal value >500 were analyzed and found to be dysregulated. The dysregulation of the striatum and that of MSN did not always correspond to each other during early stages of development (Miyazaki et al. unpublished).

1.5. Non-coding RNAs in neurodegenerative diseases

Although RNAs are related to biological phenomena such as development, differentiation and cell death, the physiological functions or expression of them in the brains have not been fully investigated. In particular, unlike protein-coding messenger RNAs (mRNAs), little is known about how many different types of ncRNAs exist, how they function, or even whether they have biological significance. Starting with the discovery of abundant and

functionally important ncRNAs including transfer RNA and ribosomal RNA in the 1950s, ncRNAs with biological roles such as *Xist* which regulates chromosome structure have been discovered (Brockdorff et al., 1992), initiating the study of long ncRNAs (lncRNAs) in the 1990s and recent years. LncRNA is a class of ncRNAs which are more than 200 nucleotides in length which do not encode proteins. This class of ncRNAs rather seem to directly function as an RNA molecule since they do not contain a functional open reading frame (ORF) (Johnson, 2012). Despite the fact that they make up the largest portion of the mammalian non-coding transcriptome and outnumber mRNAs (Esteller, 2011), the molecular functions of most of lncRNAs have remained unknown. According to previous studies, many lncRNAs may interact with various repressive chromatin regulatory complexes including PRC2, RCOR1 and SMCX (Khalil et al., 2009). Also, other lncRNAs such as *GAS5* and *NFAT* have been shown to affect the function of transcription factor (TF), either by directly binding to TF to inactivate it or by facilitating its export from the nucleus (Kino et al., 2010, Willingham et al., 2005). LncRNAs also can directly interfere with RNA polymerase II (PolII) activity and may play a role as key regulators of nuclear compartments (Kung et al., 2013). Taking these together, it can be thought that ncRNAs and their associated regulatory networks are implicated in mediating neurobiological functions, such as neurogenesis, neurotransmission, synaptic plasticity, brain aging and so on. Thus, the importance of regulatory ncRNAs in the normal functioning of CNS is becoming evident.

In addition to these features and functions of lncRNAs, there is still plenty to study about lncRNAs and their implication to neurodegenerative diseases such as HD and Alzheimer's disease (AD). Sunwoo et al. have demonstrated that lncRNAs are differentially expressed in HD and have harmful or protective effects on neuronal survival in cellular levels (Sunwoo et al., 2017), and a study has shown that the expressions of some human lncRNAs are dysregulated in HD brains (Johnson, 2012). In spite of numerous reports about HD, the link between the dysregulation of ncRNA and the pathomechanism of HD has not been fully

understood. For AD, it is suggested that alterations of ncRNA, such as *BACE1-AS* (β -secretase cleaving enzyme, antisense transcript) could contribute to risks for the disease. AD is characterized by extracellular amyloid- β ($A\beta$), intracellular neurofibrillary tangles (NFTs), and loss of synapses and neurons. The major components of senile plaques are 39-43 $A\beta$ peptide, which comes from a larger protein called amyloid precursor protein (APP). A group of secretases generates $A\beta$ from APP, and *BACE1* plays a major role in the cleavage of APP. In AD brains, both the levels and the activity of *BACE1* are increased, suggesting that *BACE1* overexpression might initiate or accelerate AD. *BACE1-AS1* enhances the stability of *BACE1* mRNA and $A\beta$ peptide accumulation through a feed-forward regulatory mechanism (Faghihi et al., 2008). These data indicate that a lncRNA could directly be implicated in the increased accumulation of APP in AD. Further studies are necessary, but it is apparent that the dysregulation of ncRNA is implicated in human neurodegenerative diseases.

In this study, from candidate ncRNAs suggested by microarray, we identify mouse ncRNAs that have homology with human ncRNAs and are assumed to be highly implicated in HD. Also, we observe the dysregulations in those ncRNA expressions and determined the localization of those ncRNAs in HD model mouse brains.

Chapter 2. Materials and Methods

Microarray: R6/2 HD model mouse that expresses Venus in MSN (R6/2 Venus mouse) was generated by crossing R6/2 mouse and *Scn4b-Venus* transgenic mouse expressing the fluorescent marker, Venus, under the control of the 9-kb *Scn4b* promoter (**Figure 2A**) (Miyazaki et al., 2014). Venus-positive cells, which indicated MSN, from the striatum of 4-week-old R6/2 Venus mice and control mice were excised and then purified by FACS (Fluorescence-activated cell sorting) at the 4-week-old in the early stages of the disease. After total RNA was extracted from MSN, complementary DNA (cDNA) was generated from the total RNA, amplified and labeled for hybridization (**Figure 2B**).

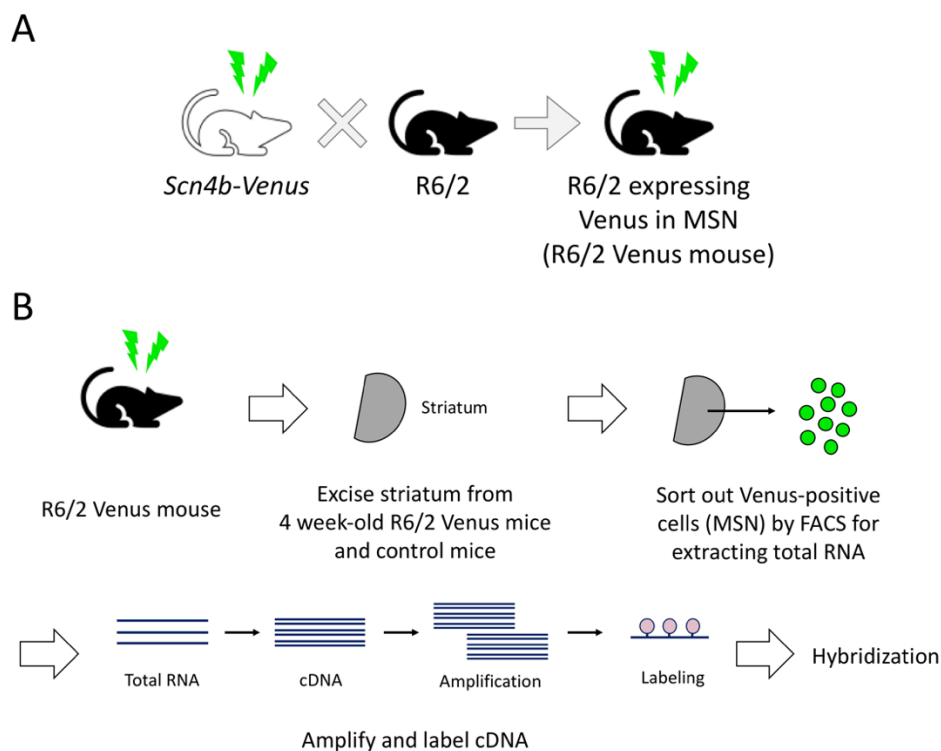


Figure 2. Schema of R6/2 Venus mouse generation and microarray analysis

Total RNA was extracted from MSN using RNeasy using RNeasy Micro (Qiagen). Generation of total cDNA from total RNA, amplification of cDNA, labeling and hybridization were performed sequentially using Ovation Pico WTA System V2 (NuGen), Genomic DNA Enzymatic Labeling Kit (Agilent), SurePrint G3 Mouse GE 8x60K Microarray Kit (Agilent).

Tissue preparation: Mice were perfused with PBS (50 ml per mouse) and 4% paraformaldehyde (PFA)/PBS (50ml per mouse). Right after brains were extracted, they were soaked in 4%PFA/PBS overnight at cold room (4°C). To prepare frozen sections, those brains were immersed in 30% sucrose solution for 2 days and 25% sucrose solution overnight at 4°C, embedded in mounting compound (TISSUE MOUNT®, Chiba Medical) and rapidly frozen in the liquid nitrogen. For conventional in situ hybridization (ISH), ViewRNA ISH and immunohistochemistry (IHC), mouse brains were sliced into sagittal and coronal sections with a cryostat (CM1860, Leica); 20 µm of thickness for conventional ISH and 12 µm of thickness for ViewRNA ISH and IHC. Mouse brain samples and frozen sections were stored at -80°C.

Quantitative real-time PCR (qRT-PCR): Ready-to-use master mix ‘FastStart Universal SYBR Green Master (Rox) (Roche)’ was used to make reaction mix. The reaction mix was placed on 96-well qRT-PCR plates, and qRT-PCR was performed on LifeCycler®480 II (Roche) as follows; 95°C for 10min (denature) → 50 cycles of 95°C for 15sec and 60°C for 1min (amplification) → 95°C for 5sec → 65°C for 1min → 95°C continuous (melting) → 40°C for 30sec (cooling). Primers are listed on **Table 1**.

Table 1. Primers for qRT-PCR

Oligo name	Oligo sequence (5' to 3')
NEAT1_1_FW/ RV	TTGGGACAGTGGACGTGTGG/ TCAAGTGCCAGCAGACAGCA
Neat1beta-RT-FW/ RV	GGGAAGGGTGTGGTCAGAAG/ GGCAGGTTGGCTCCTACAAT
Abhd11os-RT-FW/ RV	AGCATATGGTTCGAGAGCGG/ AATCCAGGAACCTTCTGCCCCG
Smim10l2a-RT-Probe-FW/ RV	TTCATGTCCCATTCTGGCCC/ GGGCACTACGGAAGACCAAA
Gm10190-RT-Probe-FW/ RV	CTCTCCATGAGGCTCTGCTG/ TCTCTTGTGCCGTTTCCC
H2-K2-RT-FW/ RV	CGACTCCAACATGGTGACCA/ TCACGCTGTGTTTCTCCTCC
Borcs8-RT-FW/ RV	AGGATCTGGGAGATGGCTT/ TGTGGATGCTGGGCTACAAG
Dleu2-New-RT-FW/ RV	GAGCCAGGTAGACACTGCTG/ GGAAGGCTCCTCCCACTTTC
Lncppara-RT-Fw/ Rv	GCTTGGCCTTCTTCTGTCT/ CCAGAGAAAGGGCTCACTGG
1300002E11Rik-RT-Fw/ Rv	TGTGAAGACCATGGCCCATC/ AGCGGGTTTAATGCAGAGCT
ZNF41-RT-Fw/ Rv	AGAGACCCTGGGAGAAGGAC/ GGCCACGTCCTTGAAGGTTA
2610316D01Rik-RT-Fw/ Rv	GGTTCAGGTTTCATCTGCCCA/ GGCACAGACATCCAGGACAA
6820431F20Rik-RT-Fw/ Rv	ATTCTGACATTGACGCCGGT/ CTGGGCTCTCTCCTCTCTGT
Gm2518-RT-Fw/ Rv	GGTGGGACTGCTAACTACC/ GGACAAACTTGCAGGCTGTG
TUNA_f/ r	ATTGGGAGGGGACTTAATGG/ GTGTTACGGAGCCAGAGAGC
BC059025_f/ r	CAGGCATTGCATTCATCAAA/AAACCTCGATATGAACAGATACACA
Tug1a-RT-FW/ RV	GAAGTGGACCTGTGACCCAG/ TGCTTGGTGAGTCGTGTCTC
Tug1b-RT-FW/ RV	GCACAGTGCTTGAAGTGCAA/ TCATCAACCACCACGGAGAC
Gapdh-RT-FW/ RV	TGTGTCCGTCGTGGATCTGA/ CCTGCTTACCACCTTCTTGA

***In situ* hybridization (ISH):** Total RNA from the striatum of 4-week-old R6/2 wild-type mouse brain was used for reverse-transcription (ReverTra Ace - α -, (Toyobo)) to amplify cDNA fragments encoding the ncRNAs (KOD Plus Neo polymerase (Toyobo)) with specific primers anchored with appropriate restriction enzyme recognition sites. Those amplified cDNAs were subcloned into pcDNA3.1/V5-HisC vector (Invitrogen) (**Figure 3A**), and the sequences were confirmed by DNA sequencing. NotI digested cDNAs were used as templates to synthesize Digoxigenin (DIG)-labeled cRNA probes (MEGAscript T7 kit (Ambion) and DIG RNA labeling Mix (Roche)) (**Figure 3B**).

Frozen sections were dried up at 42°C for 2h and cross-linked by UV illumination (1200 μ J x100) to improve stability of tissue sections and to immobilize target RNAs. The sections were incubated with PBS for 10min, postfixed with 4% formalin/PBS for 5min, washed with double distilled water, acetylated with 0.25% acetic acid/0.1 M triethanolamine (pH 8.0) for 10min and washed with PBS. The sections were first prehybridized with prehybridization solution (50% formamide/5x SSPE/0.1% SDS/ 50 mg/ml Yeast tRNA (Roche)) at 60°C for 2h then hybridized with DIG-labeled cRNA probes (1 ng cRNA probe per 200 μ l prehybridization solution) at 60°C overnight (16-18h). After the hybridization, the sections were washed twice with prewarmed (50°C) wash buffer (2x SSC/ 50% formamide) for 15min and sequentially treated at 37°C with RNaseA buffer (10 mM Tris-HCL (pH 8.0)/10 mM EDTA/0.5 M NaCl) for 15min, washed with 2x SSC wash buffer for 15min for two times and 0.2x SSC wash buffer for 15min for two times and replaced in TBST. For immunohistochemistry (IHC), the sections were incubated in Blocking Reagent (Roche) for 1h at room temperature (RT) and washed with PBS for 5min for three times. To enhance the signals, the sections were incubated with alkaline phosphatase-conjugated anti-DIG antibody (Anti-DIG-AP) diluted by Solution B (Can Get Signal Immunostain, Toyobo) for 1h at RT. After the reaction, the sections were washed with TBST for 10min for two times and NTMT (100 mM Tris-HCl (pH 9.5)/100 mM NaCl/ 50 mM

MgCl₂/0.1% Tween20) for 10min. To visualize the signals, the sections were stained with BCIP (Roche)/NBT (Roche) diluted by NTMT with 10% polyvinyl alcohol for 2-3 days at 4°C. For microscopy, the sections were washed with PBS for 20min for four times and water, dried up overnight, soaked in Xylene for 5min for three times and embedded with Mount-Quick mounting media (Daido Sangyo).

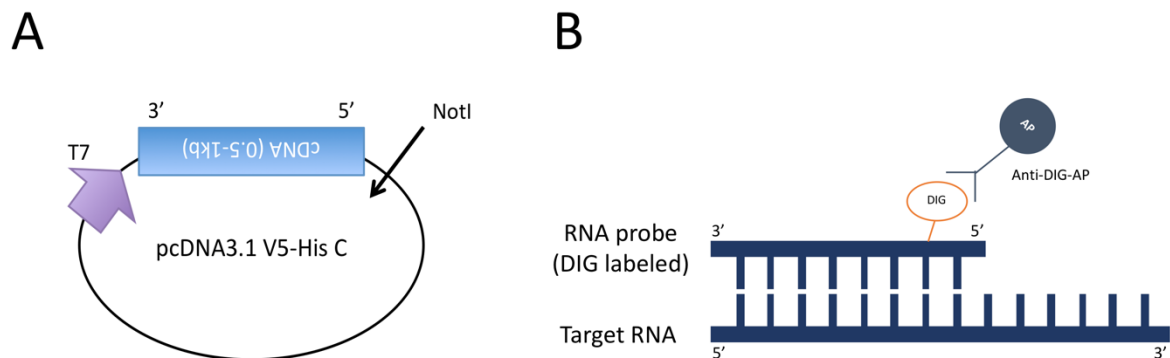


Figure 3. Construction of cRNA probe for ISH

(A) Amplified cDNAs were subcloned into pcDNA3.1/V5-HisC vector (Invitrogen), and NotI digested cDNAs were used as templates to synthesize Digoxigenin (DIG)-labeled cRNA probes (MEGAscript T7 kit (Ambion) and DIG RNA labeling Mix (Roche)). (B) DIG-labeled cRNA probe that can be detected by Anti-DIG-AP hybridizes to the target RNA.

ViewRNA ISH: Commercial ViewRNA ISH kits were used as followed: ‘ViewRNA™ ISH Tissue 1-Plex Assay Kit (Thermo Fisher Scientific)’, ‘ViewRNA Chromogenic Signal Amplification Kit (Thermo Fisher Scientific)’, and ‘ViewRNA TYPE 1 Probe Sets (Thermo Fisher Scientific)’. The target specific probes (probe assay ID: VB1-3037162-VT (*Abhd11os*), VB1-19288 (*Neat1-1*), VB1-12456-VT (*Neat1-2*), Thermo Fisher Scientific) were purchased. The probes for *Abhd11os* and *Neat1-2* were available but not for *Neat1-1*, so the probe for *Neat1-2* was designed and ordered with specific sequence that specifically detect *Neat1-2*.

Frozen sections were dried up at 42°C for 2h and incubated in prechilled 10% neutral buffered formalin (NBF) at 4°C overnight. The sections were washed with PBS for 1min, 50% ethanol, 70% ethanol, 100% ethanol for 10min each and baked at 60°C for 1h on ThermoBrite®

(Leica) with the lid open. Next, the sections were treated with Protease Set solution (3 μ l Protease QF (x100)/ 297 μ l PBS) at 40°C with the lid closed, washed with PBS for 2min for two times, postfixed with 10% NBF for 5min and washed again with PBS for 2min for two times. For hybridization, each brain section was incubated in Probe Set solution (4 μ l ViewRNA TYPE1 Probe Set/ 196 μ l Probe Set Diluent QF) for 3h at 40°C with the lid closed. After the hybridization, to amplify the signals, the sections were washed with Wash Buffer for 2min for three times, sequentially treated with PreAmp1 solution (2 μ l PreAmp1 QF/ 198 μ l Amplifier Diluent QF) for 25min at 40°C, Amp1 solution (2 μ l Amp1 QF/ 198 μ l Amplifier Diluent AF) for 15min at 40°C, Label Probe-AP solution (0.2 μ l Label Probe-AP/ 199.8 μ l Label Probe Diluent QF) for 15min at 40°C, AP Enhancer solution for 5min at RT and Fast Red Substrate solution (1/2 Fast Red Tablet/ 2.5 ml Naphthol Buffer) for 30min at 40°C (**Figure 4**). The sections were washed with Wash Buffer for 2min for three times before replacing the treatment solutions. After the signal amplification, the sections were counterstained with Mayer's Hematoxylin for 10sec and washed with water.

For microscopy, the sections were first covered with UltraMount Aqueous Permanent Mounting Medium (Dako) and incubated on ThermoBrite® (Leica) for 30min at 70°C with the lid open and embedded with HistoMount Mounting Solution (Life technologies).

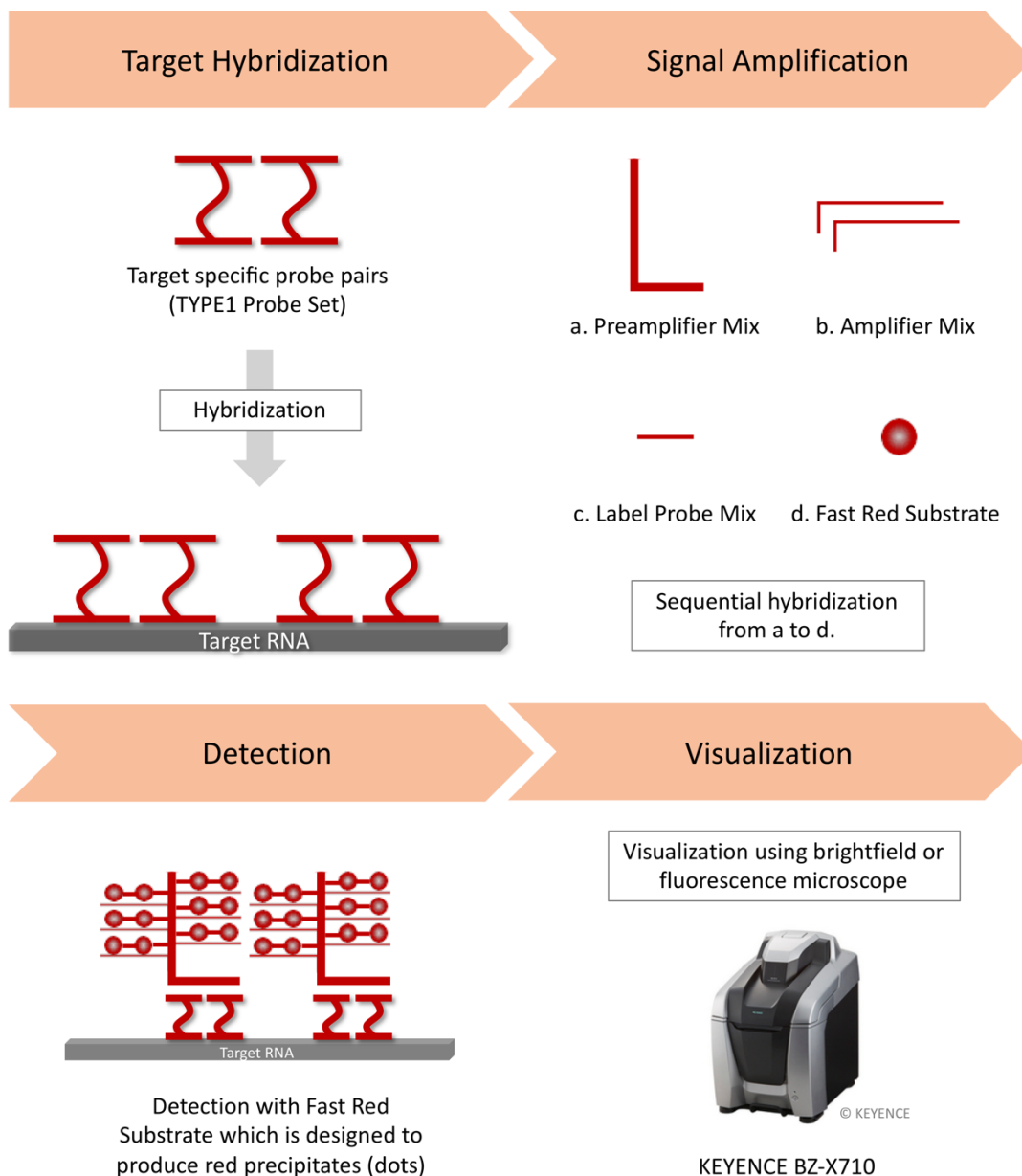


Figure 4. Workflow of ViewRNA ISH

TYPE1 probe sets are designed to provide red signals that can be visualized by both brightfield and fluorescence microscope.

IHC: For diaminobenzidine (DAB) staining, the frozen sections were incubated with PBS for 10min, postfixed with 4% formalin/ PBS for 5min and washed with water. Next, they were soaked in 0.01% Citrate buffer (0.1 M Citrate buffer/0.1M Citric sodium solution) and autoclaved for 5min at 121°C. After the activation, the sections were quenched with 100%

methanol/0.01% H₂O₂) for 30min, incubated with blocking solution (5% skim milk/TBST) for 1hr at RT and primary antibody diluted by TBST at 4°C overnight. After the secondary antibody incubation for 1h at RT, the sections were washed with TBST and incubated with VECTASTAIN Elite ABC Kit (Vector Laboratories) for 30min. To detect signals, DAB solution (10 mg DAB/ 0.5 ml 1M Tris-HCL (pH 7.6)/ 9.5 ml H₂O/ 5 µl H₂O₂, filtered) was applied to the sections for 50sec-1min, and the sections were washed with water, dried up overnight and embedded with Mount-Quick mounting media (Daido Sangyo) for microscopy.

Combined staining of ViewRNA ISH and IHC: Immunofluorescence staining was performed right after ViewRNA ISH to investigate intracellular localization of ncRNAs. After the signal amplification and detection, the Fast Red Substrate solution was removed, the sections were incubated in TBST for 5min for three times and blocking solution (5% skim milk/ TBST) for 1h at RT. After the primary antibody incubation at 4°C overnight, the sections were incubated in secondary antibody diluted by TBST and mounted with 'VECTASHEILD with DAPI (H-1200) (Vector)'. EM48 (CHEMICON, MAB5374) as an anti-htt antibody, DARPP32 as an MSN marker and anti-PSF antibody (SIGMA, P2860) that detects paraspeckles were used for investigating the intracellular localizations of ncRNAs.

Microscopy: All sections were observed via KEYENCE BZ-X710 fluorescence microscope and analyzed by BZ-X Analyzer and ImageJ.

Statistics: To examine whether the samples had the same variances, data were analyzed by *F*-test first. Outlier data were excluded by calculating with Grubb's test. All of the experiments were successfully repeated at least three times. Data were expressed as the mean ± standard error values and were analyzed with the unpaired Student's *t*-test. **p* < 0.05, ***p* < 0.01 and ****p* < 0.001. *P*-value of < 0.05 was considered statistically significant.

Chapter 3. Results

3.1. Dysregulated ncRNAs were found in the gene expression profiling data of R6/2 MSN

In order to select candidate ncRNAs, the gene expression profiling data was analyzed first. In the data, ncRNAs dysregulated in the MSN of 4-week-old R6/2 HD model mice were listed up. 4-week-old mice were used to exclude secondary effects of early dysregulated gene, since alteration of gene expression was observed at the early stage of the disease. Due to the low expression level of ncRNAs, those with fold-change (> 1.5), p-value (< 0.05) and raw signal value (> 500 , at least 1 out of 8 samples has the value within range) were considered as dysregulated ncRNAs from the data.

Among those genes, we found 52 dysregulated mouse ncRNAs, which were already registered as reference sequence in GenBank (NIH genetic sequence database) and searched the similarity between mouse and human ncRNAs sequences. Using Nucleotide BLAST provided by NCBI (National Center for Biotechnology Information), the sequences of some known mouse ncRNAs such as *Hotair*, *Xist*, *Tug1*, *Malat1* and *Meg3* were compared to the sequences of their human homologs. According to the results, the criteria of determining human homologs were diverse among mouse ncRNAs. For example, *Hotair* and its human homolog *HOTAIR* shares 84% of their sequences, and *Xist* and its human homolog *XIST* shares 67%, *Tug1* and *TUG1* shares 81%, *Malat1* and *MALAT1* shares 77%, and *Meg3* and *MEG3* shares 89% of their sequences each. Therefore, we looked for “homologs” when the sequences of mouse and human ncRNAs had more than 80% of identities with their scores more than 200. Among hundreds of mouse ncRNAs, 3 ncRNAs that met criteria were found: NR_004446 (*H2-K2*), NR_028086 (*Smim10l2a*), NR_028385 (*Gm10190*). Also, from the microarray data, 610 mouse DNA fragments with the information on their genomic coordinates were found, and 26 full-length mouse ncRNAs were identified using the UCSC (University of California Santa

Cruz) Genome Browser. From them, three ncRNAs which have homology with human ncRNAs were further selected: NR_131212 (*Neat1-2*), NR_132132 (*Borcs8*), NR_028264 (*Dleu2*). In addition to those ncRNAs, 6 dysregulated ncRNAs with scores more than 100 were added to be examined, and 3 known ncRNAs (*Abhd11os*, *Tug1* and *Tunar*) previously reported to be dysregulated in HD brains (Francelle et al., 2015, Johnson, 2012, Lin et al., 2014a) were added to confirm the reliability of the results (Table 2).

Table 2. 12 ncRNAs that were dysregulated in MSN of 4-week-old HD model mouse brains

No.	Gene symbol	Mouse ncRNA			Human ncRNA		
		FC	P	Regulation	Accession	Gene symbol	Accession
1	<i>Neat1</i>	5.18	0.002	down	NR_131212	<i>NEAT1</i>	NR_131012
2	<i>H2-K2</i>	3.05	0.022	up	NR_004446	<i>HLA-H</i>	NR_001434
3	<i>Gm10190</i>	1.67	0.015	up	NR_028385	<i>ARHGEF33</i>	NR_028386
4	<i>Borcs8</i>	2.87	0.037	down	NR_132132	<i>BORCS8-MEF2B</i>	NR_027307
5	<i>Dleu2</i>	1.66	0.036	up	NR_028264	<i>DLEU2</i>	NR_002612
6	<i>Smim10l2a</i>	1.64	0.036	up	NR_028086	<i>SMIM10L2B</i>	NR_024493
7	<i>Incppara</i>	1.61	0.038	up	NR_110483	<i>MIRLET7BHG</i>	NR_110479
8	<i>1300002E11Rik</i>	2.19	0.026	up	NR_037957	<i>MAP3K13</i>	NR_038322
9	<i>Znf41-ps</i>	2.19	0.021	up	NR_040355	<i>ZNF616</i>	NR_135823
10	<i>2610316D01Rik</i>	2.17	0.028	up	NR_045172	<i>LOC101927359</i>	NR_125885
11	<i>6820431F20Rik</i>	1.53	0.025	up	NR_030708	<i>NSFL1C</i>	NR_038164
12	<i>Gm2518</i>	4.49	0.025	up	NR_015538	<i>IFITM3</i>	NR_049759

3.2. NcRNA expressions were altered, confirmed by qRT-PCR

First, qRT-PCR was performed to examine the expression levels of these ncRNAs in the striatum and MSNs of R6/2 and control mouse. In the striatum of 4-week-old R6/2 model mouse brains, *Smim10l2a* was upregulated, and *Neat1-1*, *Neat1-2*, *H2-K2*, *Znf41-ps*, *Abhd11os* and *Tunar_v1* (a variant of *Tunar*) were downregulated (Figure 5A). In the MSN, *Neat1-1*, *Neat1-2*, *Abhd11os*, *Tug1b* and *Tunar_v1* showed downregulations (Figure 5B). *Neat1-1* and *Neat1-2* are variants of *Neat1*. Since the sequence of *Neat1-1* completely overlaps with that of *Neat1-2* (Figure 6), *Neat1-1* could not be quantified independently.

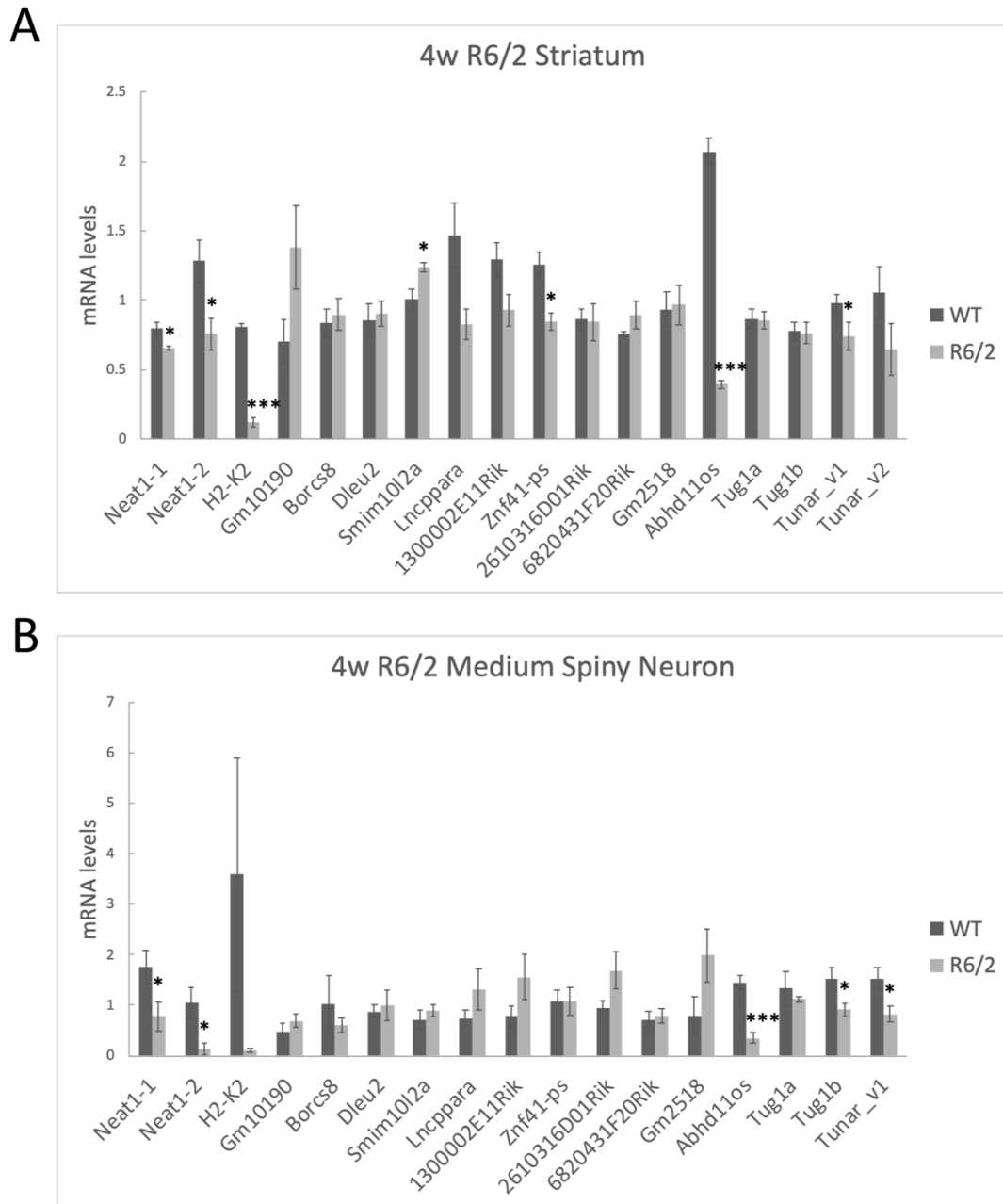


Figure 5. Verification of dysregulated ncRNAs in R6/2 striatum and MSN

qRT-PCR was performed in striatum (n=4) (A) and MSN (n=6) (B) of 4-week-old WT (wild-type littermate) and R6/2 HD model mouse brains. ‘FastStart Universal SYBR Green Master (Rox) 04 913 914 001 (Roche)’ was used as a dye for the quantification. All gene expression data were normalized to the expression levels of *Gapdh*. Data are expressed as the mean \pm standard error values. * $p < 0.05$, ** $p < 0.01$, *** $p < 0.001$.

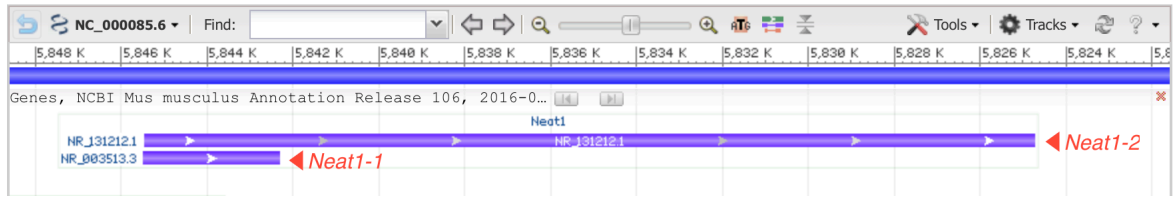


Figure 6. Two variants of *Neat1*: *Neat1-1* and *Neat1-2*

The short variant *Neat1-1* (NR_003513.3) and the long variant *Neat1-2* (NR_131212.1) completely overlaps. This information about *Neat1* is provided by NCBI.

As seen in the results (**Figure 5**), *Neat1-1*, *Neat1-2* and *Tunar_v1* were the ones that showed significant alterations in expression levels both in the striatum and MSN. On the other hand, the expression levels of *H2-K2*, *Smim10l2a*, *Znf41-ps* were altered in the striatum but not in MSN, and *Tug1b* was altered only in the MSN. Due to their low expression levels, *Tunar_v2* could not be examined in the MSN by qRT-PCR.

3.3. The dysregulation of ncRNA could not be confirmed by ISH

Next, we performed ISH (conventional ISH) on the brains of 4-week-old R6/2 and the control mice to observe the expression and to examine the localizations of the dysregulated ncRNAs. ISH is a method that allows for precise localization of a specific segment of DNA or RNA within a histological section. According to the results, however, unlike coding RNAs such as *Scn4b*, the signals of most of ncRNAs could not be detected by this method, and the alteration of their expression levels was hard to be examined due to low expression levels of those ncRNAs (**Figure 7**). Therefore, we performed ViewRNA ISH to investigate the expression changes of those poorly expressed ncRNAs by visualizing them on brain sections.

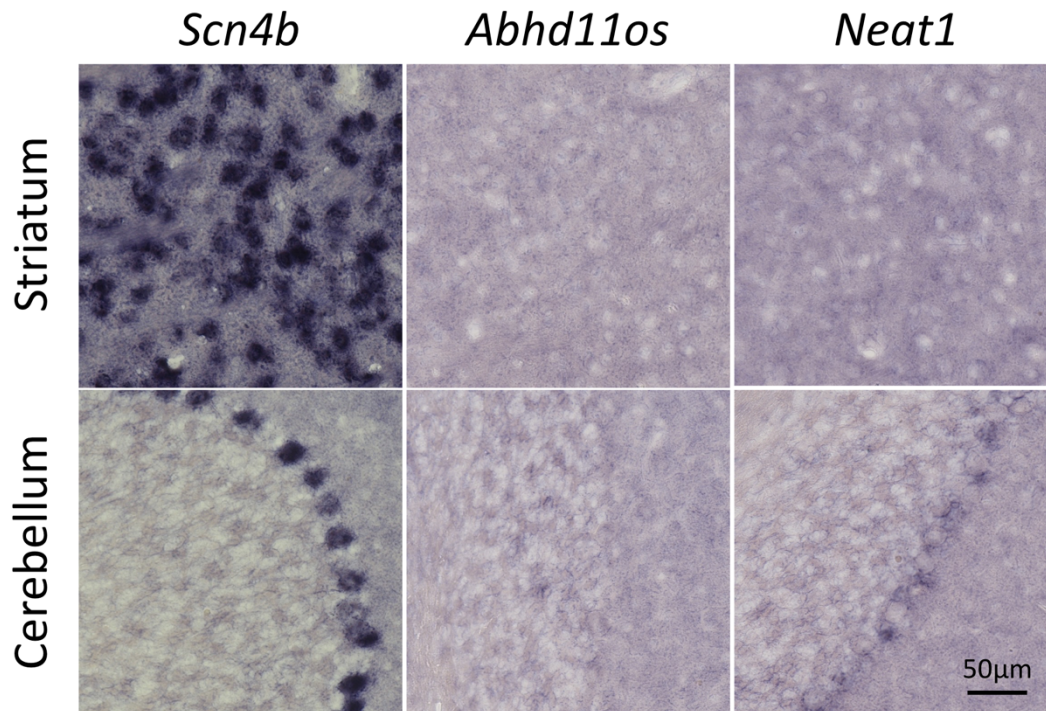


Figure 7. NcRNAs could not be detected by conventional ISH

Scn4b, a coding RNA, was detected clearly in the striatum and Purkinje cells of cerebellum. The expressions of ncRNAs *Abhd11os* and *Neat1* are ambiguous. 12-week-old B6CBA mouse brains were used.

3.4. NcRNA with low expression level was detected by ViewRNA ISH.

ViewRNA ISH provides highly specific signals and ultra-sensitive single-molecule detection of RNA, where each signal dot corresponds to one target molecule. In practice, ViewRNA ISH allowed to detect the signals of those poorly expressed ncRNAs such as *Abhd11os* that could not be detected by conventional ISH (**Figure 8**). Looking at the results of conventional ISH, it is hard to say that the expression level of *Abhd11os* was dysregulated or even was expressed in the control and R6/2 mouse brains. On the other hand, signals for *Abhd11os* were clearly detected at both control and R6/2 by ViewRNA ISH.

Also, *Scn4b*, a coding RNA which is downregulated in HD brains, was tested for sensitivity of ViewRNA ISH. *Scn4b* was detected not only in the MSN of striatum and the Purkinje cells of cerebellum strongly, but also in the hippocampal neurons (**Figure 9A**), in

which *Scn4b* was not detected by conventional ISH (Data not shown). This result suggests that ViewRNA ISH showed higher sensitivity compared to conventional ISH. Also, ViewRNA ISH clearly showed that the expression level of *Scn4b* was markedly decreased in the striatum of 4-week-old R6/2 HD mouse brains (**Figure 9B**). Taking these together, it could be said that the sensitivity of ViewRNA ISH was improved compared to the conventional ISH.

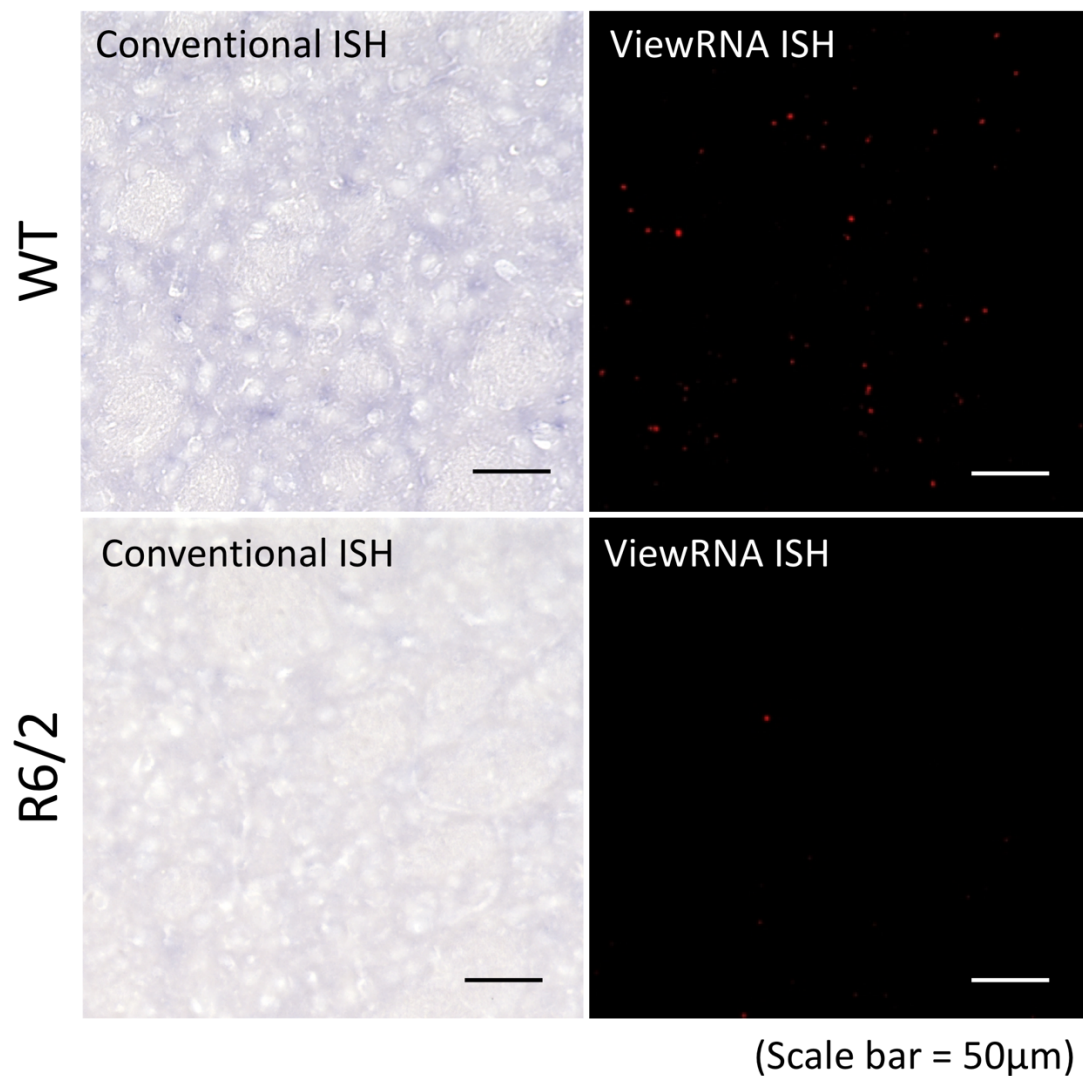
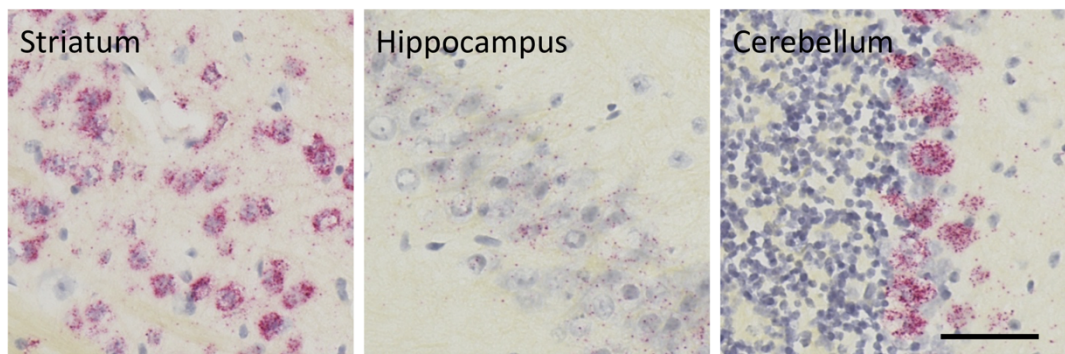


Figure 8. ViewRNA ISH allowed to detect ncRNA with low expression level

Abhd11os which could not be detected clearly by conventional ISH (left) was detected by ViewRNA ISH (right, red dots). WT; wild-type littermate.

A

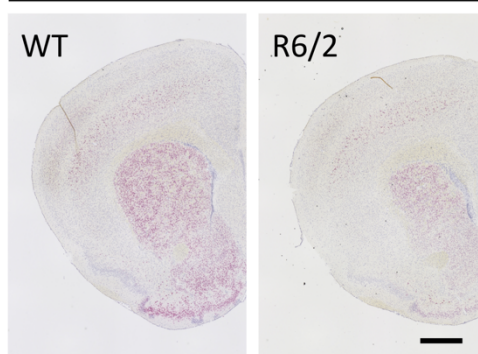
12w B6 mouse



(Scale bar = 50µm)

B

4w R6/2 HD model mouse



(Scale bar = 1,000µm)

Figure 9. ViewRNA ISH allows for precise localizations of *Scn4b*

Distribution and expression of *Scn4b* mRNA in the brain of 12-week-old B6 mouse (A, red dots) and in the striatum of 4-week-old R6/2 mouse brains (B, red dots) observed by ViewRNA ISH. In R6/2, *Scn4b* showed downregulation. WT; wild-type littermate.

3.5. Non-coding RNA *Abhd11os* and *Neat1* were downregulated in R6/2

As stated above, many ncRNAs were dysregulated in 4-week-old R6/2 HD model mouse brains. Among them, *Abhd11os* and *Neat1* were ncRNAs whose expression levels were significantly downregulated both in the R6/2 striatum and MSN (**Figure 5**). By using ViewRNA ISH, dotted *Abhd11os* and *Neat1* signals could be detected both at bright field and fluorescence images, and these signals seemed to be decreased in the striatum of R6/2 (**Figure 10**). For quantification, we counted the dotted red signals using the images of ViewRNA ISH in the striatum of R6/2 and the control. As a result, the number of *Abhd11os* signals was reduced significantly while the number of total cells remained almost the same in R6/2 (**Figure 11**). Since *Neat1* has two variants that completely overlaps (**Figure 6**), detected *Neat1-1* signals included *Neat1-2* signals. Consistent with the result of qRT-PCR, the number of *Neat1-1* and *Neat1-2* signals in the striatum of R6/2 was decreased compared to the control (**Figure 11**).

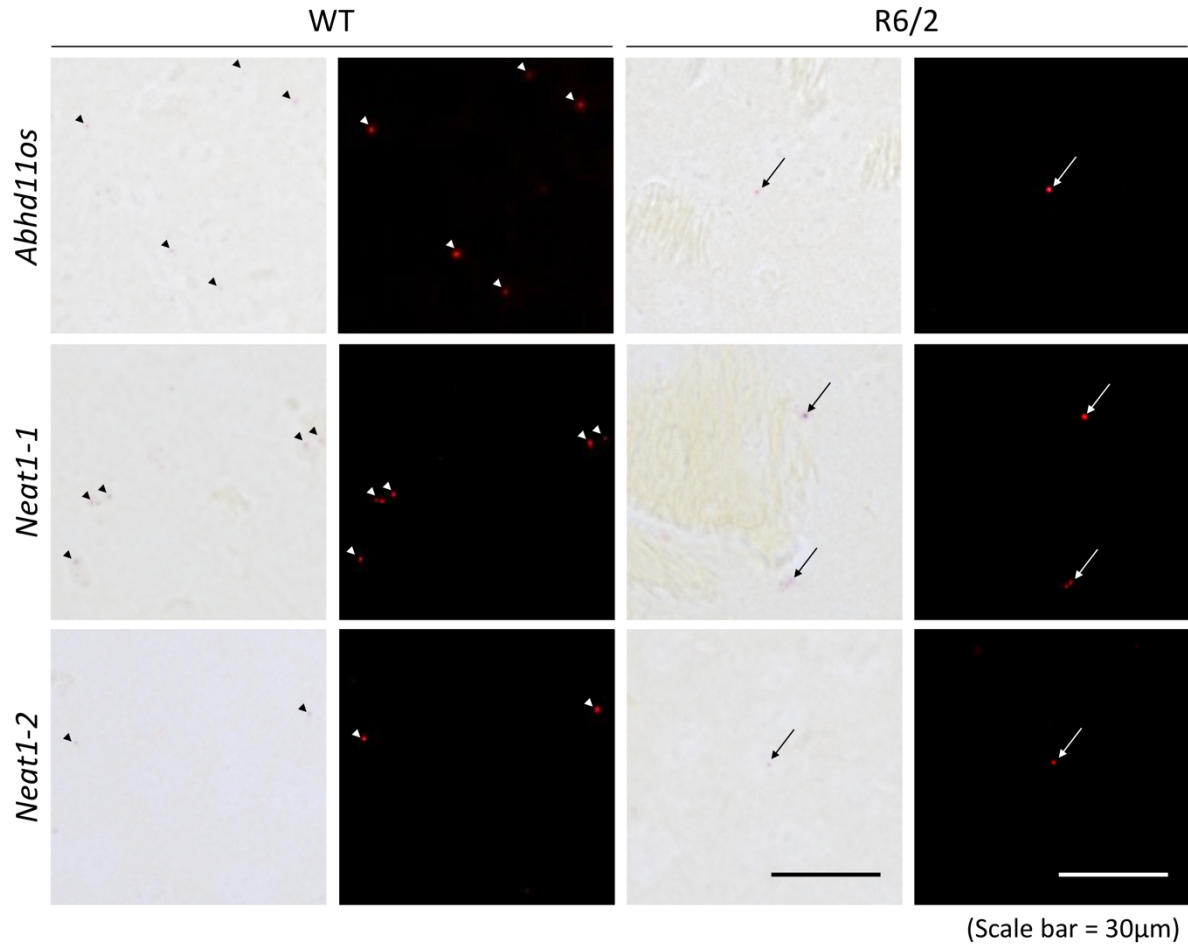


Figure 10. The signals of *Abhd11os* and *Neat1* were detected by ViewRNA ISH

ViewRNA ISH signals of *Abhd11os*, *Neat1-1* and *Neat1-2* in the striatum of 4-week-old R6/2 mouse brains. Dotted red signals were detected both at bright field and fluorescence images. Arrowheads indicate the signals in WT, and arrows indicate the signals in R6/2. WT; wild-type littermate.

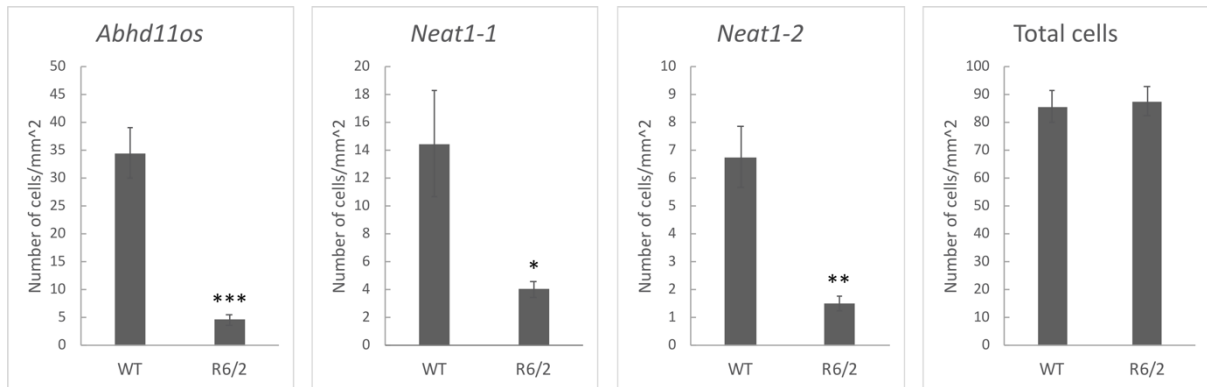


Figure 11. Quantification of dotted signals of *Abhd11os* and *Neat1* in R6/2 striatum

The number of ViewRNA ISH signals of each ncRNA and the number of total cells stained with DAPI was counted by ImageJ. Data are expressed as the mean \pm standard error values. N=3, * $p < 0.05$, ** $p < 0.01$, *** $p < 0.001$.

3.6. *Abhd11os* and *Neat1* in MSN was downregulated in R6/2

Before investigating intracellular localization of *Abhd11os* and *Neat1*, we performed double-immunostaining with EM48 (anti-htt antibody) and DARPP32 (MSN marker) to confirm the existence of mHtt in MSN of 4-week-old R6/2. EM48 is a mouse monoclonal antibody that reacts with N-terminal htt fragments (1-212 amino acids) with a normal or expanded glutamine repeat. Its immunogen is GST-fusion protein from the first 256 amino acids of human htt with a deletion of the polyQ and polyproline stretches (Gutekunst et al., 1999). The result of double-immunostaining showed that EM48 staining was detected only in R6/2 and colocalized with DARPP32, indicating that mHtt inclusions were present in MSN of R6/2 (Figure 12).

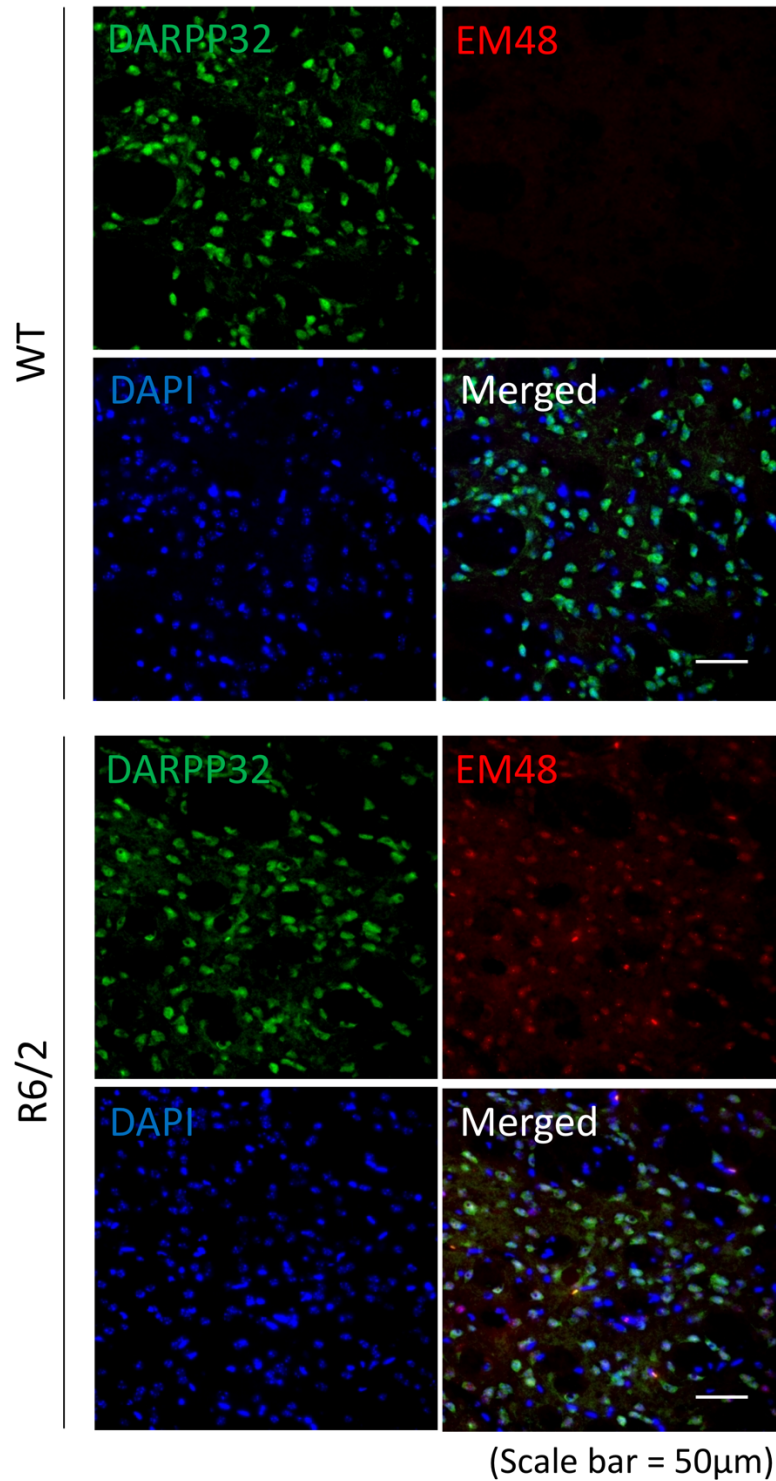


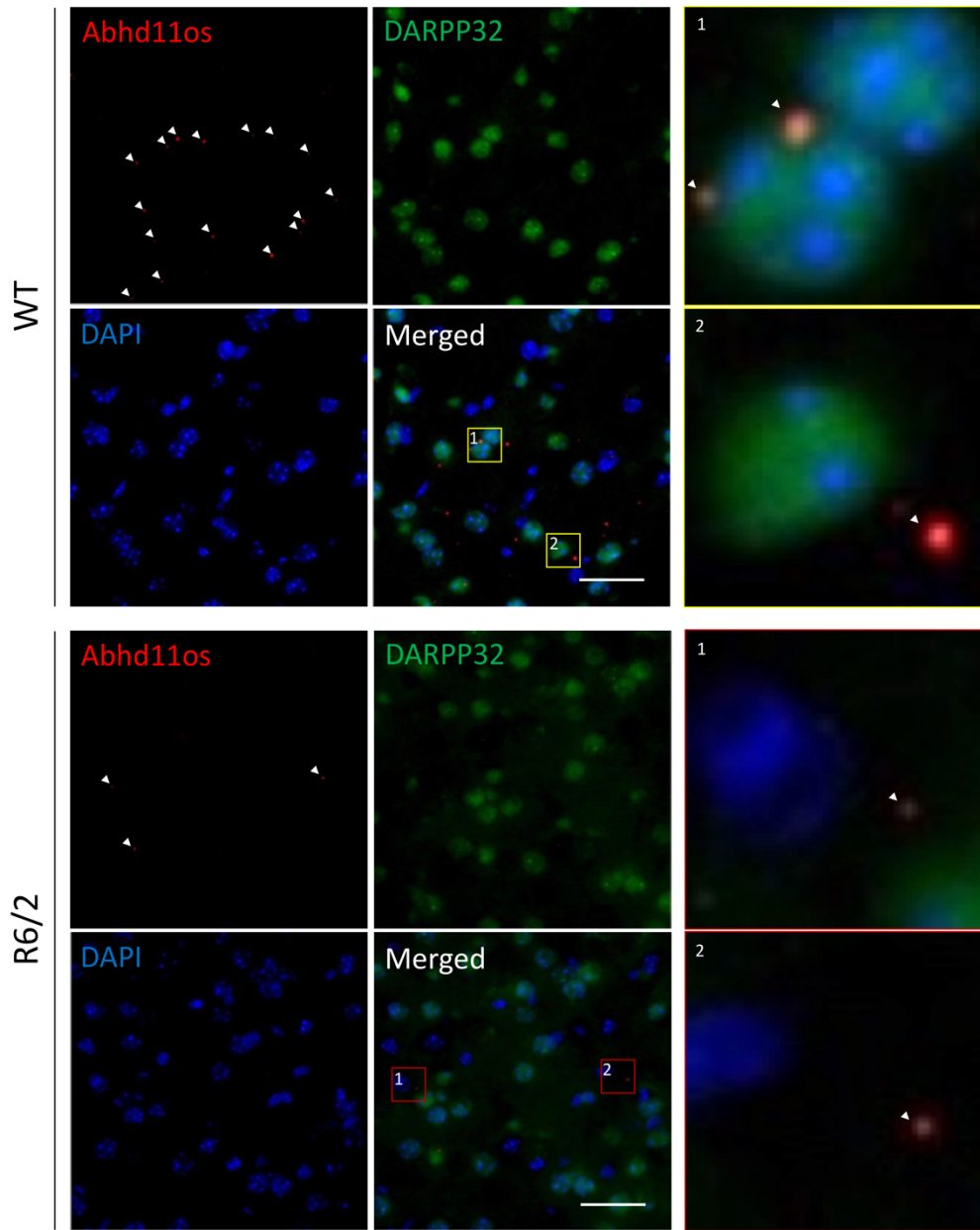
Figure 12. Mutant huntingtin is present in MSN of 4-week-old R6/2

Double-immunostaining was performed with EM48 (red, anti-htt) and DARPP32 (green, MSN marker). EM48 was detected only in R6/2 and colocalized with DARPP32. Before the primary antibody incubation, the sections were soaked in 0.01% Citrate buffer (0.1M Citrate buffer/0.1M Citric sodium solution) and autoclaved for 5min at 121°C.

Next, we performed combined staining with DARPP32 after ViewRNA ISH with *Abhd11os* probe to check whether *Abhd11os* is localized in MSNs in 4-week-old R6/2. In the control, most of *Abhd11os* signals (red, white arrowheads) were detected in DARPP32 positive cells (green), suggesting that most of *Abhd11os* were localized in MSN (**Figure 13A**). The number of *Abhd11os* signals on the DARPP32 positive cells was decreased in R6/2, while the number of DARPP32 positive cells did not change, indicating that *Abhd11os* expression was downregulated in 4-week-old R6/2 MSN (**Figure 13B**).

Similarly, ViewRNA signals of *Neat1-1* probe, which reacts with *Neat1-1* and *Neat1-2*, were mostly localized in DARPP32 positive MSN in the striatum of control mice, while it was detected mostly in DARPP32 negative and DAPI positive cells in R6/2 (**Figure 14A**). The number of *Neat1-1* probe signals in DARPP32 positive cells was significantly decreased in R6/2 (**Figure 14B**). For *Neat1-2* probe that specifically recognizes *Neat1-2*, it was more difficult to detect signals than *Neat1-1* probe both in the control and R6/2. Most of *Neat1-2* signals were observed in DARPP32 positive cells in control mice but DARPP32 negative cells in R6/2 (**Figure 14A**). The number of *Neat1-2* signals was decreased significantly in the DARPP32 positive cells in R6/2 (**Figure 14B**). Taking these together, *Neat1-1* and *Neat1-2* were downregulated in R6/2 MSN.

A



B

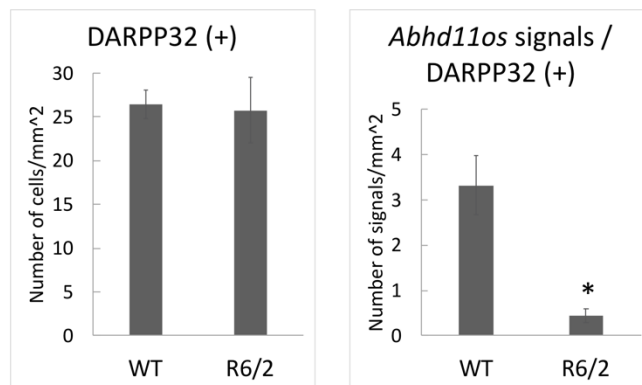


Figure 13. *Abhd11os* signals in MSN were reduced in R6/2

(A) Combined staining results of ViewRNA ISH with *Abhd11os* probe (red, arrowhead) and immunostaining with DARPP32 (green) in the striatum of 4-week-old R6/2 mouse brains and the control. Nuclei were detected by DAPI (blue) by using 'VECTASHEILD with DAPI (H-1200) (Vector)'. Box1 (yellow frame) and box2 (red frame) on the right column are the enlarged images of the cells in the merged images for providing more precise expression of the signals. (B) *Abhd11os* were downregulated in DARPP32 positive cells in R6/2. The signals were counted manually. Data are expressed as the mean \pm standard error values. N=3, * $p < 0.05$.

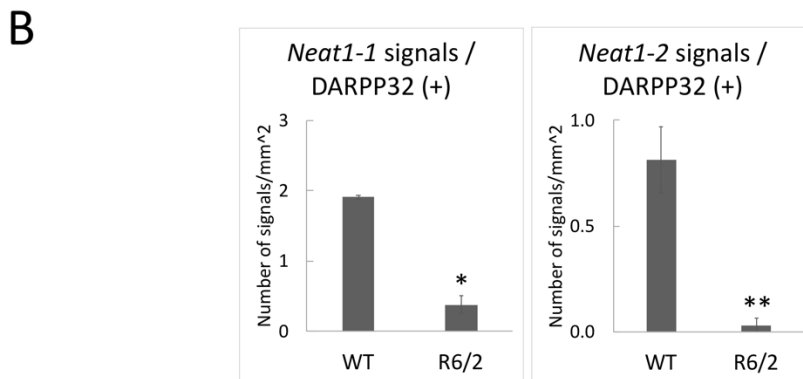
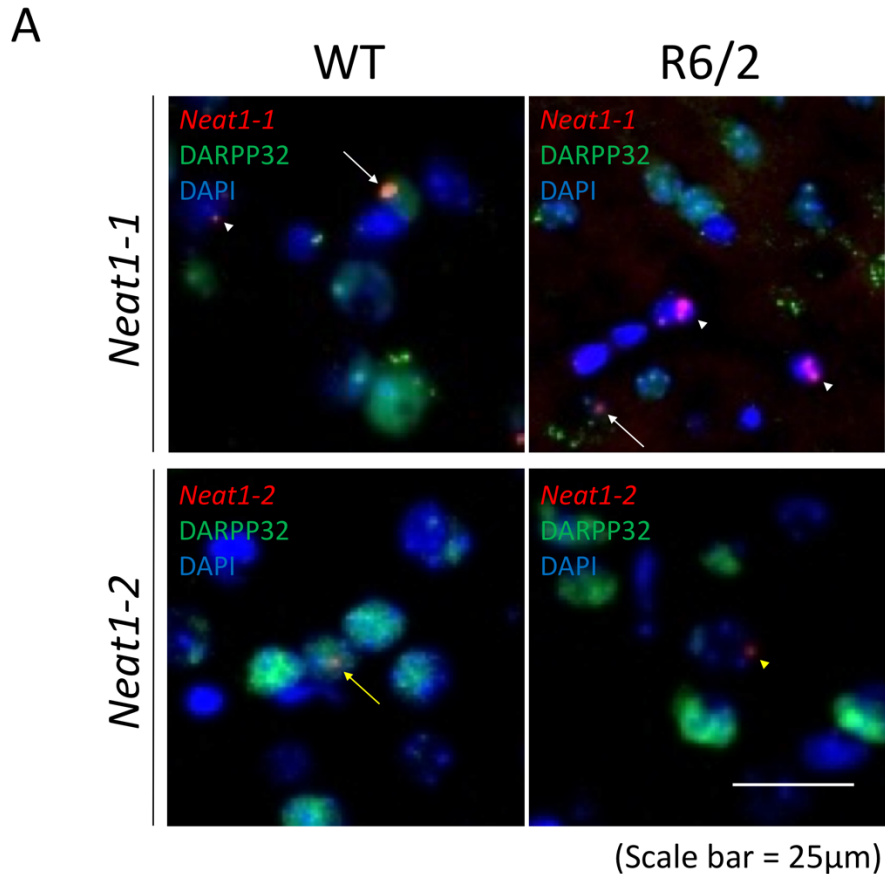


Figure 14. The signals of *Neat1-1* and *Neat1-2* in MSN were decreased in R6/2

(A) Combined staining results of ViewRNA ISH with *Neat1-1* (red, white arrow and arrowheads) or *Neat1-2* probes (red, yellow arrow and arrowhead) and immunostaining with anti-DARPP32 (green) in the striatum of 4-week-old R6/2 mouse brains and the control. The arrows indicate the signals detected in DARPP32 positive cells, and the arrowheads indicate the signals detected in DARPP32 negative cells. Nuclei were detected by DAPI (blue) by using ‘VECTASHEILD with DAPI (H-1200) (Vector)’. (B) *Neat1-1* and *Neat1-2* were downregulated in DARPP32 positive cells in R6/2. The signals were counted manually. Data are expressed as the mean \pm standard error values. N=3, * p < 0.05.

Since *Neat1* is known to associate to form paraspeckles and maintain their integrity, dysregulation of *Neat1* might affect the morphology of paraspeckles. Firstly, the localization of *Neat1* in paraspeckles was observed by using anti-PSF antibody that stains paraspeckles specifically. In the control, most of *Neat1-1* probe signals and *Neat1-2* signals were detected in DAPI positive and PSF positive cells. The red arrows indicate the signals of *Neat1-1* and *Neat1-2* which were detected in PSF positive cells, and the yellow arrowheads indicate the signals detected in DAPI positive cells without PSF staining in R6/2 (**Figure 15A**). The number of *Neat1-1* and *Neat1-2* signals were decreased in PSF staining cells (**Figure 15B**). These results suggest that most of *Neat1-1* and *Neat1-2* were downregulated in PSF positive cells in R6/2.

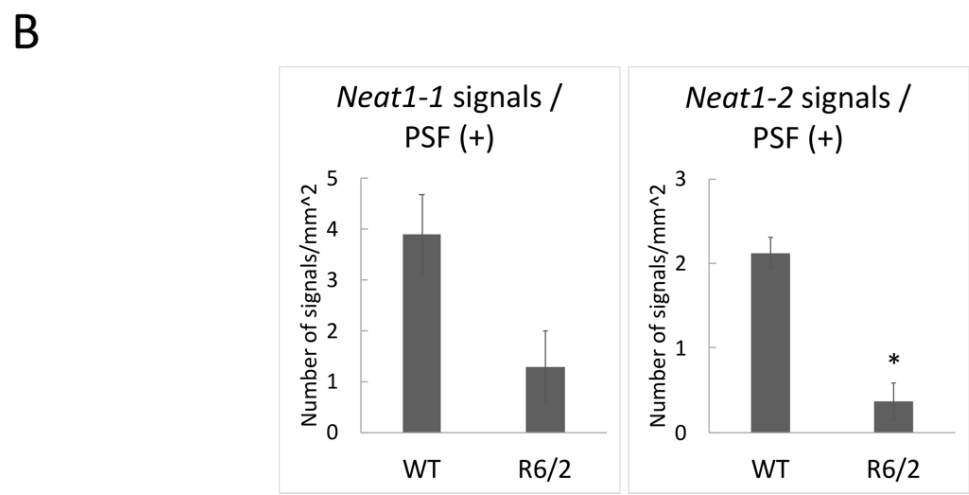
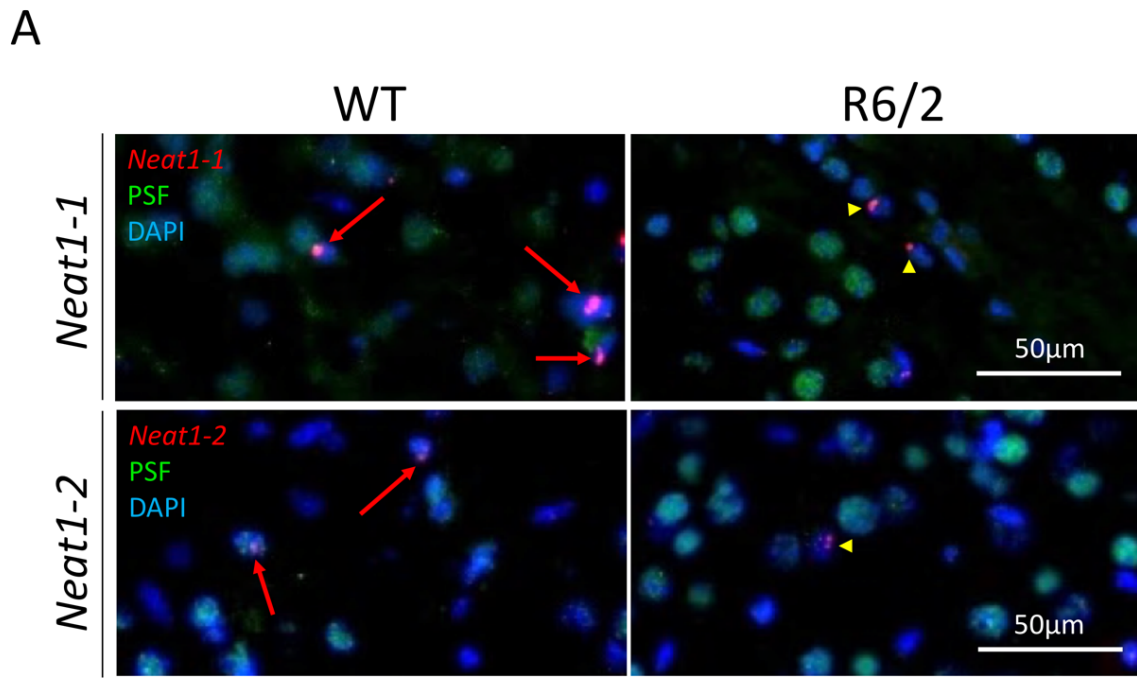


Figure 15. The signals of *Neat1-1* and *Neat1-2* localized with paraspeckles were reduced in R6/2

(A) Combined staining results of ViewRNA ISH with *Neat1-1* or *Neat1-2* probes (red) and immunostaining with anti-PSF (green) in the striatum of 4-week-old R6/2 mouse brains and the control. The red arrows indicate the signals detected in PSF positive cells, and the yellow arrowheads indicate the signals detected in PSF negative cells. Nuclei were detected by DAPI (blue) by using ‘VECTASHEILD with DAPI (H-1200) (Vector)’. (B) *Neat1-1* and *Neat1-2* were downregulated in PSF positive cells in R6/2. The signals were counted manually. Data are expressed as the mean ± standard error values. N=3, **p*< 0.05.

3.7. Dysregulation of *Neat1* might affect the morphology of paraspeckles

Neat1-1 and *Neat1-2*, which associate in forming paraspeckles in cells, were downregulated in 4-week-old R6/2 mouse brains. Also, it has been reported that specific depletion of *NEAT1-2* (human homolog of *Neat1-2*) leads to disruption of paraspeckles (Sasaki and Hirose, 2009). Therefore, it was assumed that the downregulation of *Neat1-1* and *Neat1-2* would affect paraspeckle formation in R6/2, and the number of PSF positive cells was counted because it would be reduced in R6/2 if the paraspeckle formation is affected by the reduction of *Neat1*. However, the number of PSF positive cells appeared to be increased in R6/2 (Data not shown). Instead, it became evident that the morphology of PSF positive signals in 4-week-old R6/2 striatum seemed to be more dispersed compared to the control (**Figure 16A**). The morphology of DAPI signals show no differences between R6/2 and the control (**Figure 16B**). This suggests that the loss of *Neat1-1* and *Neat1-2* in the cells might affect the formation of paraspeckles.

Taking all these together, this study revealed that the expression levels of *Abhd11os* and *Neat1* were dysregulated in MSN of presymptomatic R6/2 mice, and the disruption of *Neat1* expression might affect paraspeckle formation, which might be implicated in HD pathogenesis. The roles of ncRNA in neurodegenerative disease have not been fully understood, and it is challenging to be explored. This study suggests that ViewRNA ISH is a useful method to detect the dysregulation of ncRNAs with low expression levels, expecting to be used widely for the further studies about ncRNAs and related human diseases.

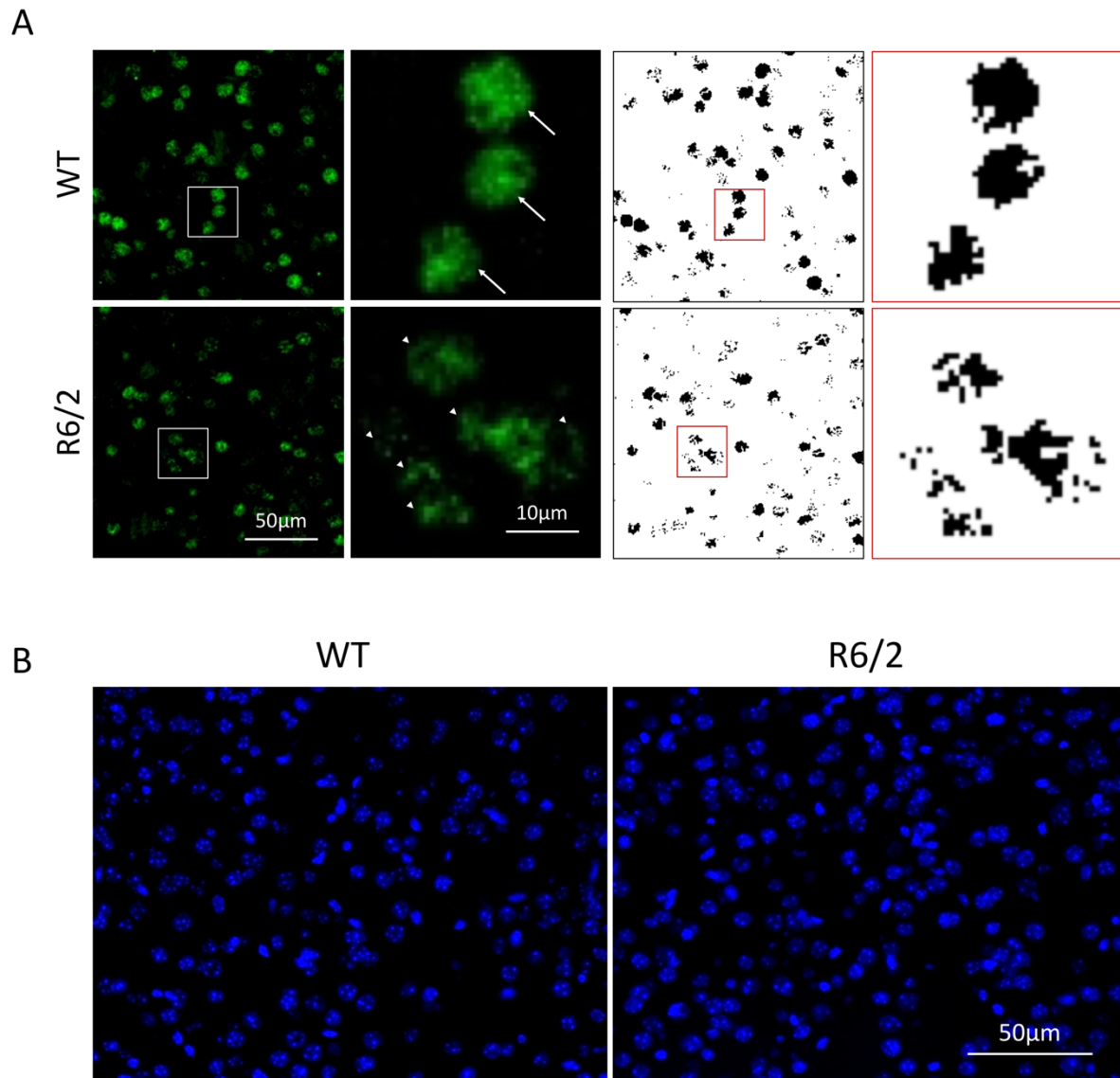


Figure 16. PSF positive signals seemed to be more dispersed in R6/2

(A) The morphology of PSF positive signals is more dispersed in R6/2 (white arrowheads) compared to the control (white arrows). Boxes on the right column are enlarged images of the anti-PSF staining. The black and white images show more clearly that the morphology of PSF positive signals is more dispersed in R6/2. (B) Double-immunostaining of anti-PSF antibody and DAPI show that DAPI staining is not changed in R6/2 compared to the control.

Chapter 4. Discussion

In this study, we found a set of ncRNAs dysregulated in MSN of 4-week-old R6/2 and explored the alteration in expression levels of those ncRNAs in the mouse brains. By using ViewRNA ISH and IHC, we showed that *Abhd11os* and *Neat1* were indeed downregulated in 4-week-old R6/2 MSN, which could not be detected by conventional ISH, suggesting that ViewRNA ISH is an effective method to evaluate RNA levels with low expressions in the brains of human disease model mice.

4.1. Non-coding RNA *Abhd11os* and HD

In this present study, we showed that the expression level of *Abhd11os* was downregulated in 4-week-old R6/2 mouse brains compared to the wild-type littermates (**Figure 5**, **Figure 10** and **Figure 11**). The intracellular localization of *Abhd11os* in R6/2 mouse brains and its downregulation within MSN were investigated by using ViewRNA ISH for the first time (**Figure 13**).

As stated above, *Abhd11os*, which is a mouse form of human *ABHD11*-antisense (Abhydrolase domain containing 11-antisense), showed the most significant alteration in expression levels in the MSN of 4-week-old R6/2. However, only little about this mouse ncRNA has been known up to date. In 2008, researchers reported that 2010001M06Rik transcript markedly downregulated in the striatum of the R6/2 HD model mouse (Brochier et al., 2008), and later, it was annotated as a long intergenic non-coding RNA (LINC00035), then renamed *ABHD11-AS1* in human and *Abhd11os* in mouse. For *Abhd11os*, a study has indicated that *Abhd11os* has a neuroprotective effect against mutant *HTT* by suggesting that it exerts a neuroprotective effect against the striatal toxicity of mutant *HTT in vivo*, whereas its downregulation exacerbates the toxicity of mutant *HTT* (Francelle et al., 2015).

In addition, recent studies about human *ABHD11* have shown that it may be implicated in many diseases such as the lipid metabolism (Arya et al., 2017), endometrial cancer (Liu et al., 2018), and ovarian cancer (Wu et al., 2017), gastric cancer (Yang et al., 2016, Lin et al., 2014b) and bladder cancer (Chen et al., 2017). Taking these together, although *Abhd11os* has not been fully investigated, and since it could be a potential modifier of mutant *HTT* toxicity (Francelle et al., 2015), *Abhd11os* may work to define novel therapeutic targets to HD.

4.2. Non-coding RNA *Neat1*, paraspeckles and HD

Neat1 is nuclear paraspeckle assembly transcript 1, which is known to associate to form paraspeckles and maintain their integrity (Bond and Fox, 2009). *NEATI*, the human homolog of *Neat1*, has two variant transcripts of 3.7kb (*NEATI-1*) and 23kb (*NEATI-2*) in length (Fox and Lamond, 2010). According to the previous studies, human *NEATI-1* alone cannot induce paraspeckle formation, and its overexpression increases the number of paraspeckles in the cells expressing *NEATI-2*. The knockdown of *NEATI-2*, however, did not affect the expression and localization of nuclear speckle markers, indicating that *NEATI-2* might not be a structural component of nuclear speckles (Clemson et al., 2009). Moreover, it was reported that specific depletion of *NEATI-2* leads to disruption of paraspeckles, and *NEATI-2* interacts with the core paraspeckle proteins gathering *NEATI-1* and other associating molecules to the periphery of paraspeckles (Sasaki and Hirose, 2009). Therefore, *NEATI-1*, rather than *NEATI-2*, might be more crucial for the formation of paraspeckles. However, in spite of their abundance within the nucleus, knockouts of either *NEATI-1* or *NEATI-2* did not have any observable phenotypic defects (Ip and Nakagawa, 2012).

Using microarray analysis and qRT-PCR, a study has revealed that *NEATI* probe, which hybridizes to both long and short variant transcripts, was upregulated in the postmortem brain of HD patients and 12-week-old R6/2 mouse brains compared to the controls (Sunwoo et al., 2017). This result is contrary to the result demonstrated in this study that *Neat1* was

downregulated in HD at the 4-week-old striatum and MSN, but there is possibility that the alterations of ncRNA expression occur in an age-dependent manner and become upside down during development. In fact, *Neat1-1* and *Neat1-2* showed no significant changes in their expression levels in 8-week-old R6/2 striatum, and H2-K2, which was downregulated in 4-week-old R6/2 striatum (**Figure 5**), was significantly upregulated in 8-week-old R6/2 striatum compared to the controls (data not shown).

Paraspeckles are a form of nuclear compartment in the interchromatin space (Fox et al., 2002), and several studies about the function of paraspeckles have indicated that paraspeckle may control RNA metabolism (Fox et al., 2005), gene expression (Prasanth et al., 2005) and transcriptional regulation (Schuldt, 2002). A recent study has demonstrated that sequestration of various paraspeckle proteins resulting from *NEAT1* upregulation might contribute to the pathogenic alteration of transcriptional status in HD, providing novel insights into the pathomechanism of the disease (Sunwoo et al., 2017). It is now necessary to define transcription factors directly affected by *NEAT1* dysregulation in HD and subsequent processes causing neuronal dysfunction and death. Despite all the efforts to reveal the HD pathogenesis, the direct link between *NEAT1* dysregulation or paraspeckle formation and the disease has not been fully elucidated yet.

In this present study, we demonstrated that paraspeckle formation is disrupted as *Neat1-1* and *Neat1-2* were downregulated in R6/2 (**Figure 16**). Since DAPI staining was not affected in R6/2, it can be thought that only paraspeckle formation was affected by the reduction of *Neat1-1* and *Neat1-2* in nucleus. Also, the relationship between the dysregulation of these ncRNAs and the formation of paraspeckles might be age-dependent, which remained to be investigated in the future. Although further studies are necessary, we suggest that the dysregulation of either *Neat1-1* or *Neat1-2* might affect the formation of paraspeckles and have potential association with HD pathogenesis, providing potential targets for developing lncRNA-based therapeutics in HD.

4.3. The effectiveness of ViewRNA ISH compared to the conventional ISH

In situ hybridization (the conventional ISH) is the technique that has widely been used to examine the localizations of RNA or DNA molecules. Basically, it involves formation of hybrid molecule between an endogenous single-stranded RNA or DNA in the cell and a complementary single-stranded RNA or DNA probe (Gall, 2016), and the probe must be labeled with something that can be detected by an antibody such as Anti-DIG-AP (**Figure 3B**). However, unlike coding RNAs such as *Scn4b*, it was difficult to detect the signals of ncRNAs and observe the expression changes of them on the brains of 4-week-old R6/2 and the control mice due to their low expression levels. As an alternative method, therefore, we used ViewRNA ISH which provides higher sensitivity to detect the signals of ncRNAs. According to the commercial guide, the probe sets are designed to consist 20 pairs of unlabeled oligos per RNA target and spans approximately 1000 bases of the target transcript to achieve maximal sensitivity. The binding of these oligo pairs to the target sequence serves as a base on which the signal amplification is built. Using multiple pairs of oligos in a single probe set ensures that there are many opportunities for the probe to bind to the target's accessible regions so as to achieve the maximal signal amplification possible for that particular RNA target molecule. Therefore, as also demonstrated in this study, this highly-sensitive ViewRNA ISH might be an effective method to evaluate RNA with low expression levels in animal samples.

4.4. Future perspectives

The contribution of ncRNAs to the genesis and progression of human diseases has attracted attention since when functional ncRNA was first discovered in 1950s. However, it has been challenging to identify all functional ncRNAs that are encoded in human genome, and much effort is now required to uncover the pathological effects of ncRNAs.

To reveal the presence and quantity of RNA, methods based on second-generation sequencing, such as RNA-seq, has been used. Although RNA-seq provides a more detailed

picture of the whole human ncRNA, it also has several informatic issues including errors in image analyses and low-quality reads. Other challenges in identifying functional ncRNAs are, for example, the lack of a complete understanding of functional motifs or domains in ncRNAs and the low expression levels of some ncRNAs. Since ncRNAs fold into complex secondary structures, sequence-based alignments alone might not be enough to identify ncRNAs (Wang et al., 2009). Nevertheless, RNA-seq is still a useful transcriptomic method and will be used to target more complex transcriptome and identify putative functional ncRNAs. ViewRNA ISH, as suggested in this study, will be one of the effective methods to help overcome those challenges by providing high-quality results of image analyses.

Further research is necessary, but it is expected that these methods will help in investigating the expression changes and understanding the functions of ncRNAs, as well as their implications to the human diseases in the future.

Chapter 5. References

1993. A novel gene containing a trinucleotide repeat that is expanded and unstable on Huntington's disease chromosomes. The Huntington's Disease Collaborative Research Group. *Cell*, 72, 971-83.
- ARYA, M., SRINIVASAN, M. & RAJASEKHARAN, R. 2017. Human alpha beta hydrolase domain containing protein 11 and its yeast homolog are lipid hydrolases. *Biochem Biophys Res Commun*, 487, 875-880.
- AUGOOD, S. J., FAULL, R. L., LOVE, D. R. & EMSON, P. C. 1996. Reduction in enkephalin and substance P messenger RNA in the striatum of early grade Huntington's disease: a detailed cellular in situ hybridization study. *Neuroscience*, 72, 1023-36.
- BAUER, P. O. & NUKINA, N. 2009. The pathogenic mechanisms of polyglutamine diseases and current therapeutic strategies. *J Neurochem*, 110, 1737-65.
- BOND, C. S. & FOX, A. H. 2009. Paraspeckles: nuclear bodies built on long noncoding RNA. *J Cell Biol*, 186, 637-44.
- BROCHIER, C., GAILLARD, M. C., DIGUET, E., CAUDY, N., DOSSAT, C., SEGURENS, B., WINCKER, P., ROZE, E., CABOCHE, J., HANTRAYE, P., BROUILLET, E., ELALOUF, J. M. & DE CHALDEE, M. 2008. Quantitative gene expression profiling of mouse brain regions reveals differential transcripts conserved in human and affected in disease models. *Physiol Genomics*, 33, 170-9.
- BROCKDORFF, N., ASHWORTH, A., KAY, G. F., MCCABE, V. M., NORRIS, D. P., COOPER, P. J., SWIFT, S. & RASTAN, S. 1992. The product of the mouse Xist gene is a 15 kb inactive X-specific transcript containing no conserved ORF and located in the nucleus. *Cell*, 71, 515-26.
- CATTANEO, E., ZUCCATO, C. & TARTARI, M. 2005. Normal huntingtin function: an alternative approach to Huntington's disease. *Nat Rev Neurosci*, 6, 919-30.
- CHAN, E. Y., LUTHI-CARTER, R., STRAND, A., SOLANO, S. M., HANSON, S. A., DEJOHN, M. M., KOOPERBERG, C., CHASE, K. O., DIFIGLIA, M., YOUNG, A. B., LEAVITT, B. R., CHA, J. H., ARONIN, N., HAYDEN, M. R. & OLSON, J. M. 2002. Increased huntingtin protein length reduces the number of polyglutamine-induced gene expression changes in mouse models of Huntington's disease. *Hum Mol Genet*, 11, 1939-51.
- CHEN, M., LI, J., ZHUANG, C. & CAI, Z. 2017. Increased lncRNA ABHD11-AS1 represses the malignant phenotypes of bladder cancer. *Oncotarget*, 8, 28176-28186.
- CLABOUGH, E. B. & ZEITLIN, S. O. 2006. Deletion of the triplet repeat encoding polyglutamine within the mouse Huntington's disease gene results in subtle behavioral/motor phenotypes in vivo and elevated levels of ATP with cellular senescence in vitro. *Hum Mol Genet*, 15, 607-23.
- CLEMSON, C. M., HUTCHINSON, J. N., SARA, S. A., ENSMINGER, A. W., FOX, A. H., CHESS, A. & LAWRENCE, J. B. 2009. An architectural role for a nuclear noncoding RNA: NEAT1 RNA is essential for the structure of paraspeckles. *Mol Cell*, 33, 717-26.
- DAVIES, S. W., TURMAINE, M., COZENS, B. A., DIFIGLIA, M., SHARP, A. H., ROSS, C. A., SCHERZINGER, E., WANKER, E. E., MANGIARINI, L. & BATES, G. P.

1997. Formation of neuronal intranuclear inclusions underlies the neurological dysfunction in mice transgenic for the HD mutation. *Cell*, 90, 537-48.
- DIFIGLIA, M., SAPP, E., CHASE, K., SCHWARZ, C., MELONI, A., YOUNG, C., MARTIN, E., VONSATTEL, J. P., CARRAWAY, R., REEVES, S. A. & ET AL. 1995. Huntingtin is a cytoplasmic protein associated with vesicles in human and rat brain neurons. *Neuron*, 14, 1075-81.
- FAGHIHI, M. A., MODARRESI, F., KHALIL, A. M., WOOD, D. E., SAHAGAN, B. G., MORGAN, T. E., FINCH, C. E., ST LAURENT, G., 3RD, KENNY, P. J. & WAHLESTEDT, C. 2008. Expression of a noncoding RNA is elevated in Alzheimer's disease and drives rapid feed-forward regulation of beta-secretase. *Nat Med*, 14, 723-30.
- FOX, A. H., BOND, C. S. & LAMOND, A. I. 2005. P54nrb forms a heterodimer with PSP1 that localizes to paraspeckles in an RNA-dependent manner. *Mol Biol Cell*, 16, 5304-15.
- FOX, A. H., LAM, Y. W., LEUNG, A. K., LYON, C. E., ANDERSEN, J., MANN, M. & LAMOND, A. I. 2002. Paraspeckles: a novel nuclear domain. *Curr Biol*, 12, 13-25.
- FOX, A. H. & LAMOND, A. I. 2010. Paraspeckles. *Cold Spring Harb Perspect Biol*, 2, a000687.
- FRANCELLE, L., GALVAN, L., GAILLARD, M. C., PETIT, F., BERNAY, B., GUILLERMIER, M., BONVENTO, G., DUFOUR, N., ELALOUF, J. M., HANTRAYE, P., DEGLON, N., DE CHALDEE, M. & BROUILLET, E. 2015. Striatal long noncoding RNA Abhd1 los is neuroprotective against an N-terminal fragment of mutant huntingtin in vivo. *Neurobiol Aging*, 36, 1601 e7-16.
- FUSCO, F. R., CHEN, Q., LAMOREAUX, W. J., FIGUEREDO-CARDENAS, G., JIAO, Y., COFFMAN, J. A., SURMEIER, D. J., HONIG, M. G., CARLOCK, L. R. & REINER, A. 1999. Cellular localization of huntingtin in striatal and cortical neurons in rats: lack of correlation with neuronal vulnerability in Huntington's disease. *J Neurosci*, 19, 1189-202.
- GALL, J. G. 2016. The origin of in situ hybridization - A personal history. *Methods*, 98, 4-9.
- GUSELLA, J. F., WEXLER, N. S., CONNEALLY, P. M., NAYLOR, S. L., ANDERSON, M. A., TANZI, R. E., WATKINS, P. C., OTTINA, K., WALLACE, M. R., SAKAGUCHI, A. Y. & ET AL. 1983. A polymorphic DNA marker genetically linked to Huntington's disease. *Nature*, 306, 234-8.
- GUTEKUNST, C. A., LI, S. H., YI, H., MULROY, J. S., KUEMMERLE, S., JONES, R., RYE, D., FERRANTE, R. J., HERSCH, S. M. & LI, X. J. 1999. Nuclear and neuropil aggregates in Huntington's disease: relationship to neuropathology. *J Neurosci*, 19, 2522-34.
- HODGES, A., STRAND, A. D., ARAGAKI, A. K., KUHN, A., SENGSTAG, T., HUGHES, G., ELLISTON, L. A., HARTOG, C., GOLDSTEIN, D. R., THU, D., HOLLINGSWORTH, Z. R., COLLIN, F., SYNEK, B., HOLMANS, P. A., YOUNG, A. B., WEXLER, N. S., DELORENZI, M., KOOPERBERG, C., AUGOOD, S. J., FAULL, R. L., OLSON, J. M., JONES, L. & LUTHI-CARTER, R. 2006. Regional and cellular gene expression changes in human Huntington's disease brain. *Hum Mol Genet*, 15, 965-77.

- HUANG, K., SANDERS, S. S., KANG, R., CARROLL, J. B., SUTTON, L., WAN, J., SINGARAJA, R., YOUNG, F. B., LIU, L., EL-HUSSEINI, A., DAVIS, N. G. & HAYDEN, M. R. 2011. Wild-type HTT modulates the enzymatic activity of the neuronal palmitoyl transferase HIP14. *Hum Mol Genet*, 20, 3356-65.
- ILLARIOSHKIN, S. N., KLYUSHNIKOV, S. A., VIGONT, V. A., SELIVERSTOV, Y. A. & KAZNACHEYEVA, E. V. 2018. Molecular Pathogenesis in Huntington's Disease. *Biochemistry (Mosc)*, 83, 1030-1039.
- IP, J. Y. & NAKAGAWA, S. 2012. Long non-coding RNAs in nuclear bodies. *Dev Growth Differ*, 54, 44-54.
- JOHNSON, R. 2012. Long non-coding RNAs in Huntington's disease neurodegeneration. *Neurobiol Dis*, 46, 245-54.
- KHALIL, A. M., GUTTMAN, M., HUARTE, M., GARBER, M., RAJ, A., RIVEA MORALES, D., THOMAS, K., PRESSER, A., BERNSTEIN, B. E., VAN OUDENAARDEN, A., REGEV, A., LANDER, E. S. & RINN, J. L. 2009. Many human large intergenic noncoding RNAs associate with chromatin-modifying complexes and affect gene expression. *Proc Natl Acad Sci U S A*, 106, 11667-72.
- KIM, M., LEE, H. S., LAFORET, G., MCINTYRE, C., MARTIN, E. J., CHANG, P., KIM, T. W., WILLIAMS, M., REDDY, P. H., TAGLE, D., BOYCE, F. M., WON, L., HELLER, A., ARONIN, N. & DIFIGLIA, M. 1999. Mutant huntingtin expression in clonal striatal cells: dissociation of inclusion formation and neuronal survival by caspase inhibition. *J Neurosci*, 19, 964-73.
- KINO, T., HURT, D. E., ICHIJO, T., NADER, N. & CHROUSOS, G. P. 2010. Noncoding RNA gas5 is a growth arrest- and starvation-associated repressor of the glucocorticoid receptor. *Sci Signal*, 3, ra8.
- KUNG, J. T., COLOGNORI, D. & LEE, J. T. 2013. Long noncoding RNAs: past, present, and future. *Genetics*, 193, 651-69.
- LIN, N., CHANG, K. Y., LI, Z., GATES, K., RANA, Z. A., DANG, J., ZHANG, D., HAN, T., YANG, C. S., CUNNINGHAM, T. J., HEAD, S. R., DUESTER, G., DONG, P. D. & RANA, T. M. 2014a. An evolutionarily conserved long noncoding RNA TUNA controls pluripotency and neural lineage commitment. *Mol Cell*, 53, 1005-19.
- LIN, X., YANG, M., XIA, T. & GUO, J. 2014b. Increased expression of long noncoding RNA ABHD11-AS1 in gastric cancer and its clinical significance. *Med Oncol*, 31, 42.
- LIU, Y., WANG, L. L., CHEN, S., ZONG, Z. H., GUAN, X. & ZHAO, Y. 2018. LncRNA ABHD11-AS1 promotes the development of endometrial carcinoma by targeting cyclin D1. *J Cell Mol Med*.
- LUTHI-CARTER, R., STRAND, A., PETERS, N. L., SOLANO, S. M., HOLLINGSWORTH, Z. R., MENON, A. S., FREY, A. S., SPEKTOR, B. S., PENNEY, E. B., SCHILLING, G., ROSS, C. A., BORCHELT, D. R., TAPSCOTT, S. J., YOUNG, A. B., CHA, J. H. & OLSON, J. M. 2000. Decreased expression of striatal signaling genes in a mouse model of Huntington's disease. *Hum Mol Genet*, 9, 1259-71.
- LUTHI-CARTER, R., STRAND, A. D., HANSON, S. A., KOOPERBERG, C., SCHILLING, G., LA SPADA, A. R., MERRY, D. E., YOUNG, A. B., ROSS, C. A., BORCHELT, D. R. & OLSON, J. M. 2002. Polyglutamine and transcription: gene expression changes shared by DRPLA and Huntington's disease mouse models reveal context-independent effects. *Hum Mol Genet*, 11, 1927-37.

- MANGIARINI, L., SATHASIVAM, K., SELLER, M., COZENS, B., HARPER, A., HETHERINGTON, C., LAWTON, M., TROTTIER, Y., LEHRACH, H., DAVIES, S. W. & BATES, G. P. 1996. Exon 1 of the HD gene with an expanded CAG repeat is sufficient to cause a progressive neurological phenotype in transgenic mice. *Cell*, 87, 493-506.
- MIYAZAKI, H., OYAMA, F., INOUE, R., AOSAKI, T., ABE, T., KIYONARI, H., KINO, Y., KUROSAWA, M., SHIMIZU, J., OGIWARA, I., YAMAKAWA, K., KOSHIMIZU, Y., FUJIYAMA, F., KANEKO, T., SHIMIZU, H., NAGATOMO, K., YAMADA, K., SHIMOGORI, T., HATTORI, N., MIURA, M. & NUKINA, N. 2014. Singular localization of sodium channel beta4 subunit in unmyelinated fibres and its role in the striatum. *Nat Commun*, 5, 5525.
- MYERS, R. H. 2004. Huntington's disease genetics. *NeuroRx*, 1, 255-62.
- NASIR, J., FLORESCO, S. B., O'KUSKY, J. R., DIEWERT, V. M., RICHMAN, J. M., ZEISLER, J., BOROWSKI, A., MARTH, J. D., PHILLIPS, A. G. & HAYDEN, M. R. 1995. Targeted disruption of the Huntington's disease gene results in embryonic lethality and behavioral and morphological changes in heterozygotes. *Cell*, 81, 811-23.
- NUCIFORA, F. C., JR., SASAKI, M., PETERS, M. F., HUANG, H., COOPER, J. K., YAMADA, M., TAKAHASHI, H., TSUJI, S., TRONCOSO, J., DAWSON, V. L., DAWSON, T. M. & ROSS, C. A. 2001. Interference by huntingtin and atrophin-1 with cbp-mediated transcription leading to cellular toxicity. *Science*, 291, 2423-8.
- OYAMA, F., MIYAZAKI, H., SAKAMOTO, N., BECQUET, C., MACHIDA, Y., KANEKO, K., UCHIKAWA, C., SUZUKI, T., KUROSAWA, M., IKEDA, T., TAMAOKA, A., SAKURAI, T. & NUKINA, N. 2006. Sodium channel beta4 subunit: down-regulation and possible involvement in neuritic degeneration in Huntington's disease transgenic mice. *J Neurochem*, 98, 518-29.
- PANDEY, M. & RAJAMMA, U. 2018. Huntington's disease: the coming of age. *J Genet*, 97, 649-664.
- PRASANTH, K. V., PRASANTH, S. G., XUAN, Z., HEARN, S., FREIER, S. M., BENNETT, C. F., ZHANG, M. Q. & SPECTOR, D. L. 2005. Regulating gene expression through RNA nuclear retention. *Cell*, 123, 249-63.
- ROSS, C. A., WOOD, J. D., SCHILLING, G., PETERS, M. F., NUCIFORA, F. C., JR., COOPER, J. K., SHARP, A. H., MARGOLIS, R. L. & BORCHELT, D. R. 1999. Polyglutamine pathogenesis. *Philos Trans R Soc Lond B Biol Sci*, 354, 1005-11.
- SASAKI, Y. T. & HIROSE, T. 2009. How to build a paraspeckle. *Genome Biol*, 10, 227.
- SAUDOU, F., FINKBEINER, S., DEVYS, D. & GREENBERG, M. E. 1998. Huntingtin acts in the nucleus to induce apoptosis but death does not correlate with the formation of intranuclear inclusions. *Cell*, 95, 55-66.
- SCHULDT, A. 2002. Proteomics of the nucleolus. *Nat Cell Biol*, 4, E35.
- SCHULTE, J. & LITTLETON, J. T. 2011. The biological function of the Huntingtin protein and its relevance to Huntington's Disease pathology. *Curr Trends Neurol*, 5, 65-78.
- SUNWOO, J. S., LEE, S. T., IM, W., LEE, M., BYUN, J. I., JUNG, K. H., PARK, K. I., JUNG, K. Y., LEE, S. K., CHU, K. & KIM, M. 2017. Altered Expression of the Long Noncoding RNA NEAT1 in Huntington's Disease. *Mol Neurobiol*, 54, 1577-1586.

- TAKANO, H. & GUSELLA, J. F. 2002. The predominantly HEAT-like motif structure of huntingtin and its association and coincident nuclear entry with dorsal, an NF- κ B/Rel/dorsal family transcription factor. *BMC Neurosci*, 3, 15.
- WANG, Z., GERSTEIN, M. & SNYDER, M. 2009. RNA-Seq: a revolutionary tool for transcriptomics. *Nat Rev Genet*, 10, 57-63.
- WEXLER, N. S. 2012. Huntington's disease: advocacy driving science. *Annu Rev Med*, 63, 1-22.
- WEXLER, N. S., LORIMER, J., PORTER, J., GOMEZ, F., MOSKOWITZ, C., SHACKELL, E., MARDER, K., PENCHASZADEH, G., ROBERTS, S. A., GAYAN, J., BROCKLEBANK, D., CHERNY, S. S., CARDON, L. R., GRAY, J., DLOUHY, S. R., WIKTORSKI, S., HODES, M. E., CONNEALLY, P. M., PENNEY, J. B., GUSELLA, J., CHA, J. H., IRIZARRY, M., ROSAS, D., HERSCH, S., HOLLINGSWORTH, Z., MACDONALD, M., YOUNG, A. B., ANDRESEN, J. M., HOUSMAN, D. E., DE YOUNG, M. M., BONILLA, E., STILLINGS, T., NEGRETTE, A., SNODGRASS, S. R., MARTINEZ-JAURRIETA, M. D., RAMOS-ARROYO, M. A., BICKHAM, J., RAMOS, J. S., MARSHALL, F., SHOULSON, I., REY, G. J., FEIGIN, A., ARNHEIM, N., ACEVEDO-CRUZ, A., ACOSTA, L., ALVIR, J., FISCHBECK, K., THOMPSON, L. M., YOUNG, A., DURE, L., O'BRIEN, C. J., PAULSEN, J., BRICKMAN, A., KRCH, D., PEERY, S., HOGARTH, P., HIGGINS, D. S., JR., LANDWEHRMEYER, B. & PROJECT, U. S.-V. C. R. 2004. Venezuelan kindreds reveal that genetic and environmental factors modulate Huntington's disease age of onset. *Proc Natl Acad Sci USA*, 101, 3498-503.
- WILLINGHAM, A. T., ORTH, A. P., BATALOV, S., PETERS, E. C., WEN, B. G., AZA-BLANC, P., HOGENESCH, J. B. & SCHULTZ, P. G. 2005. A strategy for probing the function of noncoding RNAs finds a repressor of NFAT. *Science*, 309, 1570-3.
- WU, D. D., CHEN, X., SUN, K. X., WANG, L. L., CHEN, S. & ZHAO, Y. 2017. Role of the lncRNA ABHD11-AS1 in the tumorigenesis and progression of epithelial ovarian cancer through targeted regulation of RhoC. *Mol Cancer*, 16, 138.
- YAMANAKA, T., MIYAZAKI, H., OYAMA, F., KUROSAWA, M., WASHIZU, C., DOI, H. & NUKINA, N. 2008. Mutant Huntingtin reduces HSP70 expression through the sequestration of NF-Y transcription factor. *EMBO J*, 27, 827-39.
- YANG, Y., SHAO, Y., ZHU, M., LI, Q., YANG, F., LU, X., XU, C., XIAO, B., SUN, Y. & GUO, J. 2016. Using gastric juice lncRNA-ABHD11-AS1 as a novel type of biomarker in the screening of gastric cancer. *Tumour Biol*, 37, 1183-8.
- ZUCCATO, C., CIAMMOLA, A., RIGAMONTI, D., LEAVITT, B. R., GOFFREDO, D., CONTI, L., MACDONALD, M. E., FRIEDLANDER, R. M., SILANI, V., HAYDEN, M. R., TIMMUSK, T., SIPIONE, S. & CATTANEO, E. 2001. Loss of huntingtin-mediated BDNF gene transcription in Huntington's disease. *Science*, 293, 493-8.
- ZUCCATO, C., TARTARI, M., CROTTI, A., GOFFREDO, D., VALENZA, M., CONTI, L., CATAUDELLA, T., LEAVITT, B. R., HAYDEN, M. R., TIMMUSK, T., RIGAMONTI, D. & CATTANEO, E. 2003. Huntingtin interacts with REST/NRSF to modulate the transcription of NRSE-controlled neuronal genes. *Nat Genet*, 35, 76-83.
- ZUCCATO, C., VALENZA, M. & CATTANEO, E. 2010. Molecular mechanisms and potential therapeutical targets in Huntington's disease. *Physiol Rev*, 90, 905-81.